

Upweighting Easy Samples in Fine-Tuning Mitigates Forgetting

Sunny Sanyal*, Hayden Prairie*, Rudrajit Das*, Ali Kavis*, and Sujay Sanghavi

University of Texas at Austin

{sanyal.sunny, haydenprairie, rdas}@utexas.edu, kavis@austin.utexas.edu,
sanghavi@mail.utexas.edu

Abstract

Fine-tuning a pre-trained model on a downstream task often degrades its original capabilities, a phenomenon known as “catastrophic forgetting”. This is especially an issue when one does not have access to the data and recipe used to develop the pre-trained model. Under this constraint, most existing methods for mitigating forgetting are inapplicable. To address this challenge, we propose a *sample weighting scheme for the fine-tuning data* solely based on the pre-trained model’s losses. Specifically, we upweight the easy samples on which the pre-trained model’s loss is low and vice versa to limit the drift from the pre-trained model. Our approach is orthogonal and yet complementary to existing methods; while such methods mostly operate on parameter or gradient space, we concentrate on the sample space. We theoretically analyze the impact of fine-tuning with our method in a linear setting, showing that it stalls learning in a certain subspace which inhibits overfitting to the target task. We empirically demonstrate the efficacy of our method on both language and vision tasks. As an example, when fine-tuning Gemma 2 2B on MetaMathQA, our method results in only a 0.8% drop in accuracy on GSM8K (another math dataset) compared to standard fine-tuning, while preserving 5.4% more accuracy on the pre-training datasets. Our code is publicly available at https://github.com/sanyalsunny111/FLow_finetuning.

1 Introduction

In the modern era of large-scale machine learning, one of the central goals is to design models capable of performing multiple tasks. Traditionally, this is achieved by training an appropriately large model over datasets of multiple tasks, ensuring that the model jointly learns multiple tasks at once. Unfortunately, it is not viable to repeat this process with every new additional task due to the scale of contemporary models, necessitating effective strategies that can essentially learn without full retraining. A resource-efficient convention in machine learning is to take a *pre-trained* model which is trained on some vast and diverse dataset, and *fine-tune* it on a new dataset/task. Such pre-trained models are typically large and expensive to train from scratch but perform well on a variety of tasks while offering a versatile basis for learning a new task.

Fine-tuning is a delicate process that should ideally serve multiple objectives simultaneously; we would like to use the base model and its capabilities to facilitate learning a strong model on the downstream task, and in the meantime, preserve the existing abilities of the pre-trained model. On this particular front, the major challenge in standard, unregulated fine-tuning is the *catastrophic*

*Equal contribution

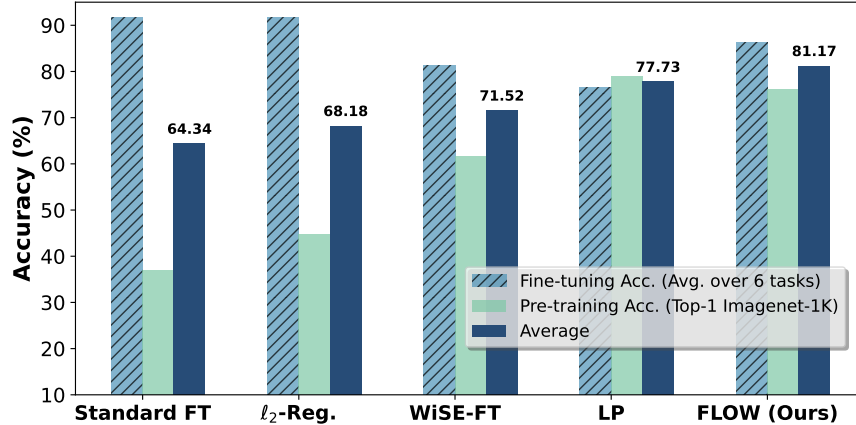


Figure 1: FLOW versus standard fine-tuning (FT) and relevant baselines for a ResNet-50 model pre-trained on ImageNet-1K (from Table 1). **FLOW achieves the best average accuracy** (between pre-training and target fine-tuning accuracies).

forgetting phenomenon. In broad terms, it describes the performance decline of the pre-trained model on previously observed data/tasks after fine-tuning on a new one. When the learning process for the downstream task interferes with the previously-learned representations beyond tolerable margins, the pre-trained model loses its prior capabilities and significantly under-performs on previously-learned tasks.

Mitigating catastrophic forgetting is an active area of research with many fundamental questions awaiting solutions. The key idea is to constrain the fine-tuning process to prevent the degeneration of the learned representations while guiding the learning of the new task to augment existing capabilities. The literature on the topic offers various approaches based on the available knowledge pertaining to the pre-training process. In fact, pre-training-specific data availability and how it is treated predominantly dictates the success of mitigating forgetting. In many real-life scenarios, however, the data and the training recipe used for generating the pre-trained model are not available [Radford et al., 2021, Touvron et al., 2023a,b, Grattafori et al., 2024, Jiang et al., 2023]. Naturally, one needs to approach the forgetting phenomenon accordingly to design realistic methods.

Therefore, we focus on the case in which we have *no access to the pre-training-specific information* during the fine-tuning process; we call it the *data-oblivious* setting. The only piece of information available during fine-tuning is indeed the pre-trained model. Therefore, one needs to devise a strategy to regulate and guide the fine-tuning process to preserve the pre-trained model capabilities while learning the new task in the absence of prior knowledge. Under this challenging setting, we present an answer to the question:

Can we design a principled method that mitigates forgetting during fine-tuning in the data-oblivious setting?

In this paper, we propose **F**ine-tuning with **P**re-trained **L**oss-**O**riented **W**eighting (**FLOW**) to mitigate catastrophic forgetting in the data-oblivious setting. Our key insight is upweighting the “easy” samples on which the pre-trained model’s loss is low and vice versa. We believe that boosting the samples on which the pre-trained model performs well (i.e., has low loss) will introduce supervised bias to the gradient updates in favor of the pre-trained model. Intuitively, this will prevent the parameters from deviating too much from the initial pre-trained state, thus mitigating forgetting.

Some prior papers assign more importance to samples with *larger losses* to accelerate the training process [Loshchilov and Hutter, 2015, Shrivastava et al., 2016, Katharopoulos and Fleuret, 2017, Kawaguchi and Lu, 2020, Das et al., 2024]. We follow the reciprocal reasoning; we tweak the fine-tuning process in favor of the pre-trained model by assigning *larger* weights to samples with *smaller* pre-trained loss values. We elaborate on this while stating our **contributions** next.

1. To mitigate forgetting, we propose **FLOW**, which fine-tunes the pre-trained model using a sample-wise weighted loss. Inspired by robust optimization ideas, we derive the i^{th} sample’s weight to be $\exp(-\ell_i/\tau)$, where ℓ_i is the i^{th} sample’s pre-trained loss and τ is a parameter which we set as $\text{median}(\ell_i)$ in practice. Thus, our method is essentially *parameter-free*.
2. We demonstrate the superiority of **FLOW** over relevant baselines (model averaging, ℓ_2 regularization, LoRA, etc.) in both vision and language model experiments. For instance, ResNet-50 fine-tuned with **FLOW** on six image classification datasets achieves $\sim 17\%$ higher average accuracy (over pre-training and fine-tuning data) than standard fine-tuning, while also surpassing other relevant baselines (see Table 1). When fine-tuning Gemma 2 2B on math datasets, the corresponding improvement of **FLOW** over standard fine-tuning is $\sim 4\%$ (see Table 2).
3. We also empirically show that combining **FLOW** with existing methods for mitigating forgetting *improves the performance* of the base methods (see Tables 3 and 4).
4. We theoretically analyze the effect of fine-tuning with **FLOW** for linear models. In particular, the covariance matrix of the fine-tuning data weighted by **FLOW** has a small eigenvalue and *training is stalled* along the corresponding eigenvector, *impeding overfitting to the fine-tuning task* (see Remark 7.4).

We end this section with a preview of the comparison of our method **FLOW** with some relevant baselines (in the data-oblivious setting) in Figure 1.

2 Related Work

2.1 Mitigating Catastrophic Forgetting

We begin by summarizing the vast literature on catastrophic forgetting with a focus on prior works most relevant to our proposed setting. For a streamlined presentation, we survey prior work in two settings – data-aware and data-oblivious. We refer the reader to Appendix A for a more detailed and explanatory literature review.

2.1.1 Data-aware approaches

The majority of the approaches for mitigating forgetting assume task-specific knowledge access to different extents; either (a subset of) the pre-training dataset itself or some information/statistic computed from pre-training data. Below, we describe the data-aware approaches based on how they make use of task-specific knowledge.

Regularization-based methods. This line of work aims to preserve existing capabilities by keeping the parameters close to the pre-trained model. The key idea is to introduce task-specific regularization to penalize modifications along the “important” directions for the old tasks [Ahn et al.,

2019]. Kirkpatrick et al. [2016] introduces the elastic weight consolidation (EWC) algorithm, which estimates the important directions by approximating the Fisher information matrix. Several variants of EWC have been proposed [Schwarz et al., 2018, Ritter et al., 2018, Lee et al., 2020, Liu et al., 2018]. Zenke et al. [2017], Aljundi et al. [2018] infer the importance of each parameter by their variational effect on the outputs. In a similar spirit, Lee et al. [2017] aims to match the posteriors of the pre-trained and fine-tuned models.

Optimization-driven methods. Another perspective to mitigating forgetting is guiding the optimization process by constraining the algorithms directly as opposed to manipulating the loss function. The core idea is to keep track of “important directions” for the old tasks, and train on the new task “orthogonally.” This could be done by storing prior data samples or gradients in a buffer [Lopez-Paz and Ranzato, 2017, Farajtabar et al., 2020, Chaudhry et al., 2019a] or by incrementally expanding the subspace of important directions without storing task-specific information [Zeng et al., 2019, Wang et al., 2021, 2023a].

Replay-based methods. A more direct approach is to store old task samples in buffers and introduce them into the training process for the new task to refresh task-specific representations periodically. There are several components to such methods. Some prior work focus on *data selection* based on the nature of old data access [Rebuffi et al., 2017, Aljundi et al., 2019, Bang et al., 2021, Chaudhry et al., 2019b, Isele and Cosgun, 2018, De Lange and Tuytelaars, 2021, Borsos et al., 2020, Tiwari et al., 2021] (e.g., streaming versus on-demand). Another important perspective is the *re-introduction strategy* of the stored information into the fine-tuning process [Silver and Mercer, 2002, Li and Hoiem, 2016, Triki et al., 2017, Lee et al., 2019a, Dhar et al., 2019, Rebuffi et al., 2017, Riemer et al., 2019, Chaudhry et al., 2019b, De Lange and Tuytelaars, 2021, Tiwari et al., 2021].

Architecture-driven methods. Another technique to limit interference between tasks is to allocate a separate trainable set of parameters per task. This could be done by initializing a sub-networks per new task [Rusu et al., 2016, Aljundi et al., 2017, Collier et al., 2020, Rajasegaran et al., 2019, Ramesh and Chaudhari, 2021, Wang et al., 2023b, 2022a], gradually expanding the parameters of a base network [Yoon et al., 2018, Ostapenko et al., 2019, Hung et al., 2019], or segregating a fixed model into task-specific subsets [Mallya et al., 2018, Kang et al., 2022, Serra et al., 2018, Wortsman et al., 2020, Mallya and Lazebnik, 2017, Mustafa B Gurbuz, 2022, Jung et al., 2020]. The main downside with this line of work is that task identities must be known for inference to (de)activate relevant sub-networks [Aljundi et al., 2017].

2.1.2 Data-oblivious approaches

In the less-explored data-oblivious setting, it is particularly challenging to devise a principled approach, as there is no access to any data-specific information, except for the pre-trained model. One line of work explores the simple idea of “model averaging” (MA) which essentially does a convex combination of the parameters of the pre-trained model and that of the fully fine-tuned model for the new task. MA and more sophisticated model merging variants have been studied in relevant context to forgetting [Lubana et al., 2021, Wortsman et al., 2021, Ilharco et al., 2023, Lin et al., 2023, Kleiman et al., 2025]. Some recent works [Chen et al., 2024a, Panda et al., 2024] introduce different strategies to selectively update a subset of parameters in a pre-training data-agnostic manner. Finally, Biderman et al. [2024] has shown that LoRA Hu et al. [2022] could be effective for mitigating catastrophic forgetting in transformers. Unlike the methods discussed above which focus

on the parameter or gradient space, ours focuses on the sample space.

2.2 Sample Selection and Weighting

Sample-wise importance selection/weighting has been studied in optimization papers [Needell et al., 2014, Zhao and Zhang, 2015, Alain et al., 2015, Stich et al., 2017] and ML papers [Loshchilov and Hutter, 2015, Shrivastava et al., 2016, Katharopoulos and Fleuret, 2017, 2018, Kawaguchi and Lu, 2020, Das et al., 2024] to speed up the optimization/training process by reducing the variance of the gradient updates. Such papers advocate focusing on “hard” samples with high-gradient norms or losses. In contrast, we focus on “easy” samples to mitigate forgetting. Another line of work focuses on robust learning under uncertain data distributions. Distributionally robust optimization (DRO) proposes to minimize the worst-case weighted loss, where the sample weights are constrained or regularized [Ben-Tal et al., 2013, Levy et al., 2020, Duchi and Namkoong, 2021, Qi et al., 2021]. Some recent works [Xie et al., 2024, Chen et al., 2024b, Anonymous, 2025] propose dynamic sample-weighting strategies for LLM training based on the previously discussed ideas.

3 Notation and Definitions

$\mathbb{1}(\cdot)$ denotes the indicator variable. For any $n \in \mathbb{N}$, the set $\{1, \dots, n\}$ is denoted by $[n]$. Vectors and matrices are in lowercase and uppercase bold font, respectively. The ℓ_p norm of a vector \mathbf{v} is denoted by $\|\mathbf{v}\|_p$. The inner product between two vectors \mathbf{v} and \mathbf{v}' is denoted as $\langle \mathbf{v}, \mathbf{v}' \rangle$. A set of n linearly independent n -dimensional vectors $\{\mathbf{u}_1, \dots, \mathbf{u}_n\}$ is said to be an orthonormal basis for \mathbb{R}^n if $\langle \mathbf{u}_i, \mathbf{u}_j \rangle = \mathbb{1}(i = j)$. A vector $\mathbf{v} = [v_1, \dots, v_n]^\top$ is said to belong to the n -dimensional probability simplex Δ_n if $\sum_{i=1}^n v_i = 1$ and $v_i \geq 0 \forall i \in [n]$. For any $n \in \mathbb{N}$, \mathbf{I}_n denotes the identity matrix of dimension n .

4 Proposed Algorithm

Our proposed algorithm consists of two main steps: (i) computing weights for the samples based on their respective pre-trained loss values; and (ii) fine-tuning with a weighted loss wherein the per-sample losses are scaled by their respective weights. The sample-wise weights are computed once and used throughout the entire fine-tuning process. We formally state our proposed fine-tuning protocol in Algorithm 1 and delve into its design details in the sequel.

Algorithm 1 Fine-tuning with Pre-trained Loss-Oriented Weighting (FLOW)

Input: Pre-trained model θ^* , dataset $\{(\mathbf{x}_i, y_i)\}_{i=1}^n$ for the new task, temperature parameter τ .

$f_i(\theta) \rightarrow i^{\text{th}}$ sample’s loss at θ , with a non-negative loss function (e.g., cross-entropy loss).

1. Compute sample weights: $w_i = \exp\left(-\frac{f_i(\theta^*)}{\tau}\right)$.
2. Weighted loss: $\mathcal{L}(\theta) = \sum_{i=1}^n w_i f_i(\theta)$.
3. Fine-tune with weighted loss: $\hat{\theta}^* := \arg \min_{\theta} \mathcal{L}(\theta)$.

Output: Fine-tuned model $\hat{\theta}^*$.

Remark 4.1. Depending on the setting, our model might have task-specific components, such as per-task prediction heads (e.g., in vision). Algorithm 1 can be slightly modified in the presence of task-specific components to enhance performance. Refer to Appendix B for these modifications.

Remark 4.2. As a heuristic prescription, we set $\tau = \text{median}(f_i(\boldsymbol{\theta}^*))$ in all our experiments (unless otherwise stated), which leads to consistently good performance. **Thus, our algorithm is essentially parameter-free in practice.**

Algorithm design. Our main intuition is that we can control forgetting by not drifting away too much from the pre-trained model (i.e., $\boldsymbol{\theta}^*$) during fine-tuning. In the presence of pre-training data, this is done by introducing data-dependent constraints on the parameter space or gradient space. Since we have *no access* to pre-training data, we redirect our focus towards *strategies on the sample space depending only on the pre-trained model*.

To that end, we propose to infer the easiness of each sample of the fine-tuning dataset with respect to the pre-trained model, based on the per-sample losses $f_i(\boldsymbol{\theta}^*)$'s (see Alg. 1). We say that the i^{th} sample is “easy” if $f_i(\boldsymbol{\theta}^*)$ is “small”.¹ Intuitively, prioritizing the “easy” samples during fine-tuning would limit the drift from $\boldsymbol{\theta}^*$. On the other hand, over-focusing on the “easy” samples would probably lead to poor performance on the fine-tuning task. Thus, it is important to strike a balance.

Let us formalize these ideas mathematically. For fine-tuning on the new task, let us consider the objective function $\mathcal{L}\boldsymbol{\pi}(\boldsymbol{\theta}) = \sum_{i=1}^n \pi_i f_i(\boldsymbol{\theta})$, where $\boldsymbol{\pi} = [\pi_1, \dots, \pi_n]^\top$ is a **static** design-choice $\in \boldsymbol{\Delta}_n$ (i.e., $\sum_{i=1}^n \pi_i = 1$ and $\pi_i \geq 0 \forall i \in [n]$) which we allow to only depend on the pre-trained model’s losses $\{f_i(\boldsymbol{\theta}^*)\}_{i=1}^n$ (and *not* the current model’s losses $\{f_i(\boldsymbol{\theta})\}_{i=1}^n$). We would like to design $\boldsymbol{\pi}$ so that:

1. for all $i \neq j$ such that $f_i(\boldsymbol{\theta}^*) \leq f_j(\boldsymbol{\theta}^*)$, $\pi_i \geq \pi_j$,
2. $\boldsymbol{\pi}$ does not concentrate around one or a few samples but rather spreads uniformly over the samples.

These two requirements can be enforced by minimizing the following function (w.r.t. $\boldsymbol{\pi}$) involving negative *entropic regularization*:

$$g(\boldsymbol{\pi}) = \sum_{i=1}^n \pi_i f_i(\boldsymbol{\theta}^*) + \tau \sum_{i=1}^n \pi_i \log \pi_i. \quad (1)$$

Here $\tau > 0$ is a parameter controlling the extent of the second requirement which is facilitated by the entropy term. We now state the minimizer of $g(\boldsymbol{\pi})$ (proof is in Appendix C).

Proposition 4.3. Let $\boldsymbol{\pi}^* = [\pi_1^*, \dots, \pi_n^*]^\top = \arg \min_{\boldsymbol{\pi} \in \boldsymbol{\Delta}_n} g(\boldsymbol{\pi})$. Then we have

$$\pi_i^* = \frac{1}{Z} \exp\left(-\frac{f_i(\boldsymbol{\theta}^*)}{\tau}\right),$$

where $Z = \sum_{j=1}^n \exp\left(-\frac{f_j(\boldsymbol{\theta}^*)}{\tau}\right)$ is the normalizing factor.

Modulo the normalizing factor Z (it does not matter when optimizing w.r.t. $\boldsymbol{\theta}$), note that w_i and $\mathcal{L}(\boldsymbol{\theta})$ in Algorithm 1 are equivalent to π_i^* and $\mathcal{L}_{\boldsymbol{\pi}^*}(\boldsymbol{\theta})$, respectively.

¹This is not a formal definition and so “small” is not quantified.

Distributionally robust optimization (DRO) perspective. Our formulation above is motivated by prior work on DRO [Qi et al., 2021], but it is **exactly the opposite** of DRO in spirit. Specifically, in our setting, Qi et al. [2021] consider the following min-max problem:

$$\min_{\boldsymbol{\theta}} \max_{\boldsymbol{\pi} \in \Delta_n} \sum_{i=1}^n \pi_i f_i(\boldsymbol{\theta}) - \tau \sum_{i=1}^n \pi_i \log \pi_i. \quad (2)$$

The first term in Eq. (2) is the *worst-case* weighted loss at $\boldsymbol{\theta}$, while the second term (i.e., entropic regularization) promotes uniform weights. The optimal solution to the inner max function w.r.t. $\boldsymbol{\pi}$ turns out to be $\pi_i^* \propto \exp\left(\frac{f_i(\boldsymbol{\theta})}{\tau}\right)$. Note that this is essentially the *inverse of our weighting function* (modulo the normalizing factor) because it assigns a higher weight to samples with larger losses (i.e., the “hard” samples). The weighting function of DRO would be very conducive to forgetting because it focuses more on the “hard” samples. Further, our weighting function is static (or one-shot) as it depends only on the losses at $\boldsymbol{\theta}^*$. On the other hand, the weighting function of DRO is dynamic (i.e., it depends on the current point $\boldsymbol{\theta}$). In fact, after plugging in the optimal value of $\boldsymbol{\pi}$ into Eq. (2) and simplifying, the DRO objective reduces to $\min_{\boldsymbol{\theta}} \sum_{i=1}^n \exp\left(\frac{f_i(\boldsymbol{\theta})}{\tau}\right)$; this is noticeably different from our objective $\mathcal{L}(\boldsymbol{\theta})$ in Algorithm 1.

5 Experimental Setup

We empirically evaluate the performance of FLOW (Algorithm 1) on vision and language tasks, showcasing its effectiveness across different model architectures and modalities. Here, we explain the details of our experiments: baselines, model architectures, datasets, and evaluation metrics.

Baselines. In our language and vision experiments, we compare FLOW against relevant baselines in the *data-oblivious setting*, namely, standard fine-tuning (fine-tuning with vanilla unweighted loss), ℓ_2 -regularization [following Kirkpatrick et al. [2016]], and WiSE-FT [Wortsman et al., 2021] (model averaging of pre-trained and standard fine-tuned models). Additionally, we compare against linear probing (fine-tuning only the classification head, keeping the body frozen) in vision experiments and low-rank adaptation (LoRA) [Hu et al., 2022] in language experiments. More details on baselines can be found in Appendix G.1.

5.1 Vision Experiments

We study the performance of FLOW and associated baselines in a transfer learning setup.

Models. We consider ResNet-18 and ResNet-50 models pre-trained on Imagenet-1K [Russakovsky et al., 2015] taken from Wightman et al. [workshop].

Datasets. We select six widely-used image classification datasets: CIFAR-10 [Krizhevsky, 2009], CIFAR-100 [Krizhevsky, 2009], Flowers102 [Nilsback and Zisserman, 2008], Caltech101 [Li et al., 2022], Cars [Krause et al., 2013], and Dogs [Parkhi et al., 2012].

Evaluation metrics. Vision models are trained with task-specific parts, such as classification head (head) and batch-norm (BN); see Appendix B for how FLOW works with with task-specific

Table 1: **Performance of FLOW with vision models.** **Bolded** and underlined values indicate the **best** and second-best accuracies within each column (and for each model). Deltas (in color) for IN-1K and target performance are computed w.r.t. the pre-trained and standard fine-tuned models. **FLOW attains the best average accuracy** and is better than the second-best method (linear probing) by 2.94% and 3.44% for ResNet-18 and ResNet-50, respectively.

	Method	IN-1K Acc.	Target Acc.	Average
ResNet-18	Pre-trained	69.76 (+0.00)	–	–
	Standard FT	19.58 (-50.18)	89.07 (+0.00)	54.60
	Linear Probe	69.76 (+0.00)	73.57 (-15.50)	<u>71.63</u>
	ℓ_2 -Reg.	34.78 (-34.98)	<u>88.12</u> (-0.95)	61.45
	WiSE-FT	54.15 (-15.61)	80.23 (-8.84)	67.19
	FLOW (Ours)	<u>65.21</u> (-4.55)	83.93 (-5.14)	74.57
ResNet-50	Pre-trained	79.02 (+0.00)	–	–
	Standard FT	36.91 (-42.11)	91.78 (+0.00)	64.34
	Linear Probe	79.02 (+0.00)	76.45 (-15.33)	<u>77.73</u>
	ℓ_2 -Reg.	44.78 (-34.24)	<u>91.58</u> (-0.20)	68.18
	WiSE-FT	61.65 (-17.37)	81.38 (-10.40)	71.52
	FLOW (Ours)	<u>76.09</u> (-2.93)	86.25 (-5.53)	81.17

parts. Forgetting is measured by how much the model’s top-1 validation accuracy on ImageNet-1K (subsequently referred to as IN-1K accuracy) reduces after fine-tuning. We report the fine-tuning performance in terms of *average fine-tuning accuracy* over all the six datasets following Goyal et al. [2023], Ilharco et al. [2023]. For IN-1K evaluation *after* fine-tuning, we replace the task-specific components of the fine-tuned model with their pre-trained counterparts. An extended discussion on experimental details, evaluation, and hyper-parameters are in Appendix G.4. We also report the **average** of IN-1K accuracy and averaged fine-tuning accuracy for each method; this is a reasonable *unified metric* to evaluate the performance of a method jointly on the pre-training and fine-tuning data.

5.2 Language Model Experiments

We follow a similar setup to Biderman et al. [2024], Chen et al. [2024a], where a language model’s general capabilities are evaluated before and after fine-tuning on a mathematical reasoning dataset. All training for language experiments is done with HuggingFace `peft` [Mangrulkar et al., 2022], `transformers` [Wolf et al., 2020], `datasets` [Lhoest et al., 2021], and `accelerate` [Gugger et al., 2022].

Models. We use Gemma 2 2B [Team et al., 2024] and Llama 3.2 3B [Grattafiori et al., 2024] as our base language models. Further details on training hyper-parameters can be found in Appendix G.2.

Datasets. Following previous works [Biderman et al., 2024, Chen et al., 2024a], we fine-tune on MetaMathQA [Yu et al., 2023], a mathematical reasoning dataset that is bootstrapped from the training set of GSM8K [Cobbe et al., 2021] and MATH [Hendrycks et al., 2021a] using a LLM. We train with all 395K samples in MetaMathQA.

Table 2: **Performance of FLOW with LLMs.** After fine-tuning Gemma 2 2B and Llama 3.2 3B on MetaMathQA, we compare the target fine-tuning performance (GSM8K) with general capability performance. **Bolded** and underlined values indicate the **best** and second-best results within each column (and for each model). Deltas (in color) for general capability metrics and fine-tuning metrics are computed w.r.t. the pre-trained and standard fine-tuned model’s accuracy, respectively. We see that **FLOW, on average, has the best performance** on general capabilities and target domain, achieving within $\sim 0.8\%$ (Gemma 2 2B) and $\sim 1.4\%$ (Llama 3.2 3B) of standard fine-tuning’s target performance, while significantly mitigating the degradation of general pre-training capabilities in comparison to other baselines.

Method		General Capability Acc.			Target Acc.	Average
		Commonsense	MMLU	MBPP	GSM8K	
Gemma 2 2B	Pre-trained	<u>57.23</u> (+0.00)	49.59 (+0.00)	28.40 (+0.00)	24.49 (-38.89)	40.79
	Standard Fine-tuning	55.07 (-2.16)	45.59 (-4.00)	16.80 (-11.60)	63.38 (+0.00)	46.31
	WiSE-FT ($\alpha = 0.5$)	57.28 (+0.05)	50.13 (+0.54)	25.60 (-2.80)	53.30 (-10.08)	47.60
	LoRA ($r = 64$)	55.67 (-1.56)	44.28 (-5.31)	25.80 (-2.60)	60.43 (-2.95)	47.05
	ℓ_2 -Regularization	57.01 (-0.22)	48.43 (-1.16)	24.80 (-3.60)	<u>62.85</u> (-0.53)	<u>49.19</u>
	FLOW (Ours)	57.59 (+0.36)	49.31 (-0.28)	<u>26.80</u> (-1.60)	62.55 (-0.83)	49.98
Llama 3.2 3B	Pre-trained	<u>54.48</u> (+0.00)	54.34 (+0.00)	38.00 (+0.00)	26.01 (-40.94)	44.28
	Standard Fine-tuning	50.68 (-3.80)	45.29 (-9.05)	17.80 (-20.20)	66.95 (+0.00)	46.10
	WiSE-FT ($\alpha = 0.5$)	54.54 (+0.04)	53.33 (-1.01)	34.60 (-3.40)	57.01 (-9.94)	50.75
	LoRA ($r = 64$)	53.10 (-1.38)	50.95 (-3.39)	34.00 (-4.00)	63.84 (-3.15)	51.66
	ℓ_2 -Regularization	53.60 (-0.88)	51.28 (-3.06)	33.60 (-4.40)	<u>66.87</u> (-0.08)	<u>52.30</u>
	FLOW (Ours)	54.30 (-0.18)	51.86 (-2.48)	<u>36.00</u> (-2.00)	65.58 (-1.37)	52.87

Evaluation metrics. To evaluate the validity of FLOW, we break down our metrics into *general capability* and *target fine-tuning* evaluations. To evaluate general capabilities, we again follow a similar setup as Chen et al. [2024a], where we use commonsense reasoning, 5-shot MMLU [Hendrycks et al., 2021b], and 3-shot MBPP [Austin et al., 2021] metrics. To evaluate the target domain, we use 5-shot GSM8K [Cobbe et al., 2021]. All evaluations are performed with `lm-evaluation-harness` [Gao et al., 2024]. More details on evaluation and the commonsense metric can be found in Appendix G.3. Similar to vision, we also report the **average** of general capabilities and the target fine-tuning accuracies as a *unified metric*.

6 Experimental Results

6.1 Comparing FLOW and Related Baselines

For **vision** experiments, Table 1 lists the accuracies of all the baselines and FLOW. Our findings are consistent among the two vision models, so we focus on the larger ResNet-50 model. The pre-trained ResNet-50 model achieves a top-1 accuracy of 79.02% on ImageNet-1K’s validation set. Standard fine-tuning experiences a significant 42.11% drop in IN-1K accuracy, while achieving an average fine-tuning accuracy of 91.78% across the target datasets. In contrast, FLOW suffers only a 2.93% drop in IN-1K accuracy and exhibits a reasonable 86.25% average accuracy on target fine-tuning datasets, demonstrating a significant improvement over standard fine-tuning. Overall, FLOW’s **average** on IN-1K and target domain accuracy is **16.83% higher** than standard fine-tuning.

Table 3: **WiSE-FT with FLOW vs. (standalone) WiSE-FT in vision.** “WiSE-FT+” denotes WiSE-FT with FLOW in the table. Comparison here is in the same setting as Table 1. Note that **WiSE-FT+ is significantly better than WiSE-FT.**

	Method	IN-1K Acc.	Target Acc.	Average
ResNet-18	WiSE-FT	54.15	80.23	67.19
	WiSE-FT+	68.71	74.03	71.37
ResNet-50	WiSE-FT	61.65	81.38	71.52
	WiSE-FT+	78.29	73.80	76.04

Table 4: **ℓ_2 -Reg./LoRA with FLOW vs. (standalone) ℓ_2 -Reg./LoRA in language.** “ ℓ_2+ ” and “LoRA+” denote ℓ_2 -Reg. with FLOW and LoRA with FLOW, respectively. The results below are for Gemma 2 2B in the same setup as Table 2. We let A1, A2, A3, and B1 represent Commonsense, MMLU, MBPP, and GSM8K, respectively. We see that **ℓ_2+ and LoRA+ are better than ℓ_2 and LoRA.**

Method	A1	A2	A3	B1	Avg.
ℓ_2	57.01	48.43	24.80	62.85	49.19
ℓ_2+	57.53	49.38	26.60	62.02	49.79
LoRA	55.67	44.28	25.80	60.43	47.05
LoRA+	56.74	47.68	28.80	61.49	49.31

Going beyond standard fine-tuning, our results in Table 1 show that FLOW comprehensively outperforms other baselines. Interestingly, despite its simplicity, linear probing is the second-best method. Overall, FLOW outperforms other baselines, when **averaging** IN-1K and target fine-tuning accuracies, by a **3.44% advantage** over the closest competitor, linear probing. Although linear probing completely prevents forgetting, it learns significantly less during fine-tuning compared to FLOW. The accuracies on individual fine-tuning datasets and corresponding accuracies for IN-1K can be found in Appendix H.

Our **language model** results are in Table 2. Results for Gemma 2 2B show that FLOW helps preserve (and even somewhat enhance) the general capabilities of the pre-trained model. Specifically, compared to standard fine-tuning, FLOW improves general capability accuracy by 2.52% in commonsense reasoning, 3.73% in MMLU, and 10.00% in MBPP, with a minor degradation of 0.83% in GSM8K. We see a similar trend in our Llama 3.2 3B experiments. Furthermore, while alternative baselines show specific strengths (such as WiSE-FT’s general capability performance and ℓ_2 -regularization’s target fine-tuning performance), **FLOW outperforms all baselines, on average**, for both models, striking the best balance between preserving general capabilities and achieving good target fine-tuning performance. Additional details on commonsense reasoning results are in Appendix I.1 and an ablation for our choice of sample weighting in LLMs is in Appendix I.2.

In summary, *FLOW strikes a good balance between learning a new task and retaining knowledge from pre-training.*

6.2 Combining FLOW with Related Baselines

To complement our results in Tables 1 and 2, we investigate the performance of baselines when **combined with FLOW**. In the vision setting, we consider uniform model averaging with WiSE-FT (with $\alpha = 0.5$) and report its performance with and without FLOW in Table 3. Interestingly, averaging the pre-trained IN-1K model and the fine-tuned model obtained with FLOW **improves** over standard WiSE-FT (i.e., averaging the pre-trained IN-1K model and the standard fine-tuned model) by **4.18%** and **4.52%** for ResNet-18 and ResNet-50, respectively, in average performance.

Further, as seen in Table 4, FLOW **boosts the performance** of other baselines in language modeling. When combined with ℓ_2 -regularization, we observe improvements in general capability between 0.5% and 1.80%, with only a 0.83% reduction in GSM8K performance. Furthermore, the integration of FLOW with LoRA yields even stronger results, enhancing general capability performance by 1.07% to 3.40%, while simultaneously improving GSM8K performance by 1.06%. Further details and discussion combining FLOW with ℓ_2 -regularization and LoRA are in Appendix I.1.

7 Theoretical Analysis

Here we consider linear pre-training and fine-tuning tasks² and theoretically analyze the effect of fine-tuning with our proposed method FLOW (Algorithm 1). Specifically, we compare the non-asymptotic trajectories of FLOW and vanilla fine-tuning. A key insight of our analysis is that FLOW stalls training in a certain direction, impeding overfitting to the fine-tuning task (see Remark 7.4). We also demonstrate that FLOW goes beyond the simple idea of model averaging (see Remark 7.5).

We begin by describing the problem setting.

Pre-training task: The label $y \in \mathbb{R}$ for a d -dimensional data point $\mathbf{x} \sim \mathcal{P}$ is given by $y = \langle \boldsymbol{\theta}_*, \mathbf{x} \rangle$, where $\boldsymbol{\theta}_* \in \mathbb{R}^d$ is the ground-truth model. Let \mathcal{D} denote the joint distribution of (\mathbf{x}, y) , where $\mathbf{x} \sim \mathcal{P}$. Let $\boldsymbol{\Sigma} = \mathbb{E}_{\mathbf{x} \sim \mathcal{P}}[\mathbf{x}\mathbf{x}^\top]$ be the data covariance matrix. Without loss of generality, let $\boldsymbol{\Sigma} \succeq \mathbf{I}_d$.

Fine-tuning task: The label $\tilde{y} \in \mathbb{R}$ for a d -dimensional data point $\tilde{\mathbf{x}} \sim \tilde{\mathcal{P}}$ is given by $\tilde{y} = \langle \tilde{\boldsymbol{\theta}}_*, \tilde{\mathbf{x}} \rangle$, where $\tilde{\boldsymbol{\theta}}_* \in \mathbb{R}^d$ is the ground-truth model. Let $\tilde{\mathcal{D}}$ denote the joint distribution of $(\tilde{\mathbf{x}}, \tilde{y})$, where $\tilde{\mathbf{x}} \sim \tilde{\mathcal{P}}$. Also, let

$$\mathbf{e} := \boldsymbol{\theta}_* - \tilde{\boldsymbol{\theta}}_*, \quad \bar{\mathbf{e}} := \frac{\mathbf{e}}{\|\mathbf{e}\|_2},$$

and $\bar{\mathbf{e}}_\perp$ be a unit vector orthogonal to $\bar{\mathbf{e}}$. We consider the case of $\tilde{\mathcal{P}} = \mathcal{N}(\vec{\mathbf{0}}_d, \tilde{\boldsymbol{\Sigma}})$, where

$$\tilde{\boldsymbol{\Sigma}} = \mathbf{I}_d + \rho(\bar{\mathbf{e}}\bar{\mathbf{e}}^\top + \bar{\mathbf{e}}_\perp\bar{\mathbf{e}}_\perp^\top), \quad (3)$$

where $\rho \in [0, 1)$ is a constant. Note that $\tilde{\boldsymbol{\Sigma}}$ is the data covariance matrix here.

Remark 7.1 (Regarding $\tilde{\boldsymbol{\Sigma}}$). *We study the case of $\tilde{\boldsymbol{\Sigma}}$ as given in Eq. (3) because it is the minimal analytically tractable case where we can show that FLOW goes beyond model averaging (MA) (see Remark 7.5). Specifically, if $\rho = 0$ and $\tilde{\boldsymbol{\Sigma}} = \mathbf{I}_d$, then FLOW reduces to MA. Moreover, for an arbitrary $\tilde{\boldsymbol{\Sigma}}$, characterizing the eigen-spectrum of the matrix dictating the trajectory of FLOW becomes intractable. For the analysis to be tractable, we need some relationship between $\tilde{\boldsymbol{\Sigma}}$ and \mathbf{e} (i.e., the difference between the optima of the pre-training and fine-tuning tasks).*³

²Our insights carry over to neural networks following the dynamics of linear models under gradient descent [Lee et al., 2019b].

³See Appendix E for more details.

For a model parameterized by $\boldsymbol{\theta} \in \mathbb{R}^d$, let

$$\begin{aligned}\text{err}_1(\boldsymbol{\theta}) &:= \mathbb{E}_{\mathcal{D}} \left[(y - \langle \boldsymbol{\theta}, \mathbf{x} \rangle)^2 \right] = (\boldsymbol{\theta} - \boldsymbol{\theta}_*)^\top \boldsymbol{\Sigma} (\boldsymbol{\theta} - \boldsymbol{\theta}_*), \\ \text{err}_2(\boldsymbol{\theta}) &:= \mathbb{E}_{\tilde{\mathcal{D}}} \left[(\tilde{y} - \langle \boldsymbol{\theta}, \tilde{\mathbf{x}} \rangle)^2 \right] = (\boldsymbol{\theta} - \tilde{\boldsymbol{\theta}}_*)^\top \tilde{\boldsymbol{\Sigma}} (\boldsymbol{\theta} - \tilde{\boldsymbol{\theta}}_*)\end{aligned}\quad (4)$$

be the population errors on the pre-training and fine-tuning tasks, respectively. Also, the total error with $\boldsymbol{\theta}$ on the two tasks is denoted by $\text{err}_{\text{tot}}(\boldsymbol{\theta}) = \text{err}_1(\boldsymbol{\theta}) + \text{err}_2(\boldsymbol{\theta})$.

We assume that initially, we learn $\boldsymbol{\theta}_*$ with the pre-training data; so $\boldsymbol{\theta}_*$ is our pre-trained model. Note that

$$\text{err}_{\text{tot}}(\boldsymbol{\theta}_*) = \text{err}_2(\boldsymbol{\theta}_*) = \mathbf{e}^\top \tilde{\boldsymbol{\Sigma}} \mathbf{e} = \|\mathbf{e}\|_2^2, \quad (5)$$

where the last step follows by using $\tilde{\boldsymbol{\Sigma}}$ from Equation (3).

We start fine-tuning starting from $\boldsymbol{\theta}_*$. Specifically, we assume access to the population $(\tilde{\mathbf{x}}, \tilde{y}) \sim \tilde{\mathcal{D}}$ of the fine-tuning task, but we lose access to the pre-training data.

Vanilla fine-tuning (FT): We minimize $\text{err}_2(\boldsymbol{\theta})$ (Eq. (4)) with gradient descent (GD) starting from $\boldsymbol{\theta}_*$ using a constant learning rate $\bar{\eta}$. Our iterate $\bar{\boldsymbol{\theta}}_K$ at the K^{th} iteration is given by (using the value of $\tilde{\boldsymbol{\Sigma}}$ from Eq. (3) and $\boldsymbol{\theta}_* - \tilde{\boldsymbol{\theta}}_* = \mathbf{e}$):

$$\bar{\boldsymbol{\theta}}_K = \tilde{\boldsymbol{\theta}}_* + \left(\mathbf{I}_d - 2\bar{\eta} \left(\mathbf{I}_d + \rho(\bar{\mathbf{e}}\bar{\mathbf{e}}^\top + \bar{\mathbf{e}}_\perp\bar{\mathbf{e}}_\perp^\top) \right) \right)^K \mathbf{e}. \quad (6)$$

FLOW: For some temperature τ , the weight of $(\tilde{\mathbf{x}}, \tilde{y}) \sim \tilde{\mathcal{D}}$ is $w(\tilde{\mathbf{x}}, \tilde{y}) = \exp\left(-\frac{(\tilde{y} - \langle \boldsymbol{\theta}_*, \tilde{\mathbf{x}} \rangle)^2}{\tau}\right)$. We minimize

$$\widehat{\text{err}}_2(\hat{\boldsymbol{\theta}}) := \mathbb{E}_{\tilde{\mathcal{D}}} \left[w(\tilde{\mathbf{x}}, \tilde{y}) (\tilde{y} - \langle \hat{\boldsymbol{\theta}}, \tilde{\mathbf{x}} \rangle)^2 \right], \quad (7)$$

with GD starting from $\boldsymbol{\theta}_*$ using a constant learning rate $\hat{\eta}$. Suppose our iterate at the K^{th} iteration is $\hat{\boldsymbol{\theta}}_K$.

Theorem 7.2 (FLOW). *Let $\mu = \left(\frac{\tau}{\tau + 2\|\mathbf{e}\|_2^2}\right)^{1/2}$. Then:*

$$\hat{\boldsymbol{\theta}}_K = \tilde{\boldsymbol{\theta}}_* + \left(\mathbf{I}_d - 2\hat{\eta}\tilde{\boldsymbol{\Sigma}}' \right)^K \mathbf{e}, \quad (8)$$

where $\tilde{\boldsymbol{\Sigma}}' := \mu(\mathbf{I}_d - \mathbf{Q})$ with

$$\mathbf{Q} = (1 - \mu^2)\bar{\mathbf{e}}\bar{\mathbf{e}}^\top + \rho^2(1 - \mu^2)\bar{\mathbf{e}}_\perp\bar{\mathbf{e}}_\perp^\top - \rho\mu^2(\bar{\mathbf{e}}\bar{\mathbf{e}}^\top + \bar{\mathbf{e}}_\perp\bar{\mathbf{e}}_\perp^\top). \quad (9)$$

We prove Theorem 7.2 in Appendix D. The **main technical challenge** is the evaluation of $\tilde{\boldsymbol{\Sigma}}'$, viz., the covariance matrix of the **weighted** fine-tuning data; see Lemma F.1 for this.

Now, we are going to compare vanilla FT (6) with $\bar{\eta} = \frac{1}{2}$ and FLOW (8) with $\hat{\eta} = \frac{1}{2\mu}$. We believe these are comparable learning rates for vanilla FT and FLOW because the resultant matrices (Eqs. (10) and (11)) dictating the convergence of both methods have exactly two non-zero eigenvalues and the corresponding eigenvectors lie in the span of $\bar{\mathbf{e}}$ and $\bar{\mathbf{e}}_\perp$. Plugging in $\bar{\eta} = \frac{1}{2}$ into Eq. (6), we get:

$$\bar{\boldsymbol{\theta}}_K = \tilde{\boldsymbol{\theta}}_* + \mathbf{P}^K \mathbf{e}, \quad \text{with } \mathbf{P} = -\rho(\bar{\mathbf{e}}\bar{\mathbf{e}}^\top + \bar{\mathbf{e}}_\perp\bar{\mathbf{e}}_\perp^\top) \quad (10)$$

for vanilla FT. Plugging in $\hat{\eta} = \frac{1}{2\mu}$ into Eq. (8), we get:

$$\hat{\boldsymbol{\theta}}_K = \tilde{\boldsymbol{\theta}}_* + \mathbf{Q}^K \mathbf{e}, \text{ with } \mathbf{Q} \text{ given by Eq. (9)} \quad (11)$$

for FLOW. The non-zero eigenvalues of \mathbf{P} are $\mp\rho$ and the corresponding eigenvectors are $\frac{1}{\sqrt{2}}(\bar{\mathbf{e}} \pm \bar{\mathbf{e}}_\perp)$. Using this in (10) and simplifying, we get for vanilla FT:

$$\bar{\boldsymbol{\theta}}_K = \tilde{\boldsymbol{\theta}}_* + \rho^K \left(\mathbf{1}(K \text{ is even})\mathbf{e} - \mathbf{1}(K \text{ is odd})\|\mathbf{e}\|_2\bar{\mathbf{e}}_\perp \right). \quad (12)$$

Remark 7.3 (Vanilla FT). *Since $\rho < 1$, $\bar{\boldsymbol{\theta}}_K$ converges to $\tilde{\boldsymbol{\theta}}_*$ rapidly, and we cannot impede this convergence.*

Note that (we use $\boldsymbol{\Sigma} \succeq \mathbf{I}_d$ below):

$$\text{err}_{\text{tot}}(\tilde{\boldsymbol{\theta}}_*) = \text{err}_1(\tilde{\boldsymbol{\theta}}_*) = \mathbf{e}^\top \boldsymbol{\Sigma} \mathbf{e} \geq \|\mathbf{e}\|_2^2. \quad (13)$$

On the other hand, the non-zero eigenvalues and corresponding eigenvectors of \mathbf{Q} are not as straightforward to compute. We do this computation in Lemma F.3 with the re-parameterization of $\mu = \sqrt{\frac{\beta(1-\rho^2)}{(1+\beta)(1-\beta\rho^2)}}$ for some $\beta \in (0, 1]$.⁴ Using this in Eq. (11) and simplifying, we get for FLOW:

$$\hat{\boldsymbol{\theta}}_K = \tilde{\boldsymbol{\theta}}_* + \left(\frac{\hat{\lambda}_1^K + \hat{\lambda}_2^K \beta^2 \rho^2}{1 + \beta^2 \rho^2} \right) \mathbf{e} - \beta \rho \left(\frac{\hat{\lambda}_1^K - \hat{\lambda}_2^K}{1 + \beta^2 \rho^2} \right) \|\mathbf{e}\|_2 \bar{\mathbf{e}}_\perp, \quad (14)$$

where $\hat{\lambda}_1 = \frac{1+\beta\rho^2}{1+\beta}$ and $\hat{\lambda}_2 = \rho^2 \left(\frac{1-\beta}{1-\beta\rho^2} \right)$.

Remark 7.4 (FLOW's trajectory). *Note that we can control $\hat{\lambda}_1$ by varying β . Specifically, we can make $\hat{\lambda}_1$ arbitrarily close to 1 by choosing a small enough β . On the other hand, $\frac{1-\beta}{1-\beta\rho^2} < \frac{1+\beta\rho^2}{1+\beta} = \hat{\lambda}_1$ and so, $\hat{\lambda}_2 < \rho^2 \hat{\lambda}_1$. Hence, beyond a certain number of iterations K , Eq. (14) effectively becomes:*

$$\hat{\boldsymbol{\theta}}_K \approx \boldsymbol{\theta}_K := \tilde{\boldsymbol{\theta}}_* + \gamma(K, \beta) \left(\mathbf{e} - \beta \rho \|\mathbf{e}\|_2 \bar{\mathbf{e}}_\perp \right), \quad (15)$$

with $\gamma(K, \beta) := \left(\frac{\hat{\lambda}_1^K}{1 + \beta^2 \rho^2} \right)$. Because we can control $\hat{\lambda}_1$ by varying β , we can control $\gamma(K, \beta)$. Thus, we can stall convergence along $(\mathbf{e} - \beta \rho \|\mathbf{e}\|_2 \bar{\mathbf{e}}_\perp)$, impeding the convergence of $\hat{\boldsymbol{\theta}}_K$ to $\tilde{\boldsymbol{\theta}}_*$.

The direction $(\mathbf{e} - \beta \rho \|\mathbf{e}\|_2 \bar{\mathbf{e}}_\perp)$ is the eigenvector of \mathbf{Q} with the largest eigenvalue (see Lemma F.3). Since $\tilde{\boldsymbol{\Sigma}}' = \mu(\mathbf{I}_d - \mathbf{Q})$ (recall $\tilde{\boldsymbol{\Sigma}}'$ is the covariance matrix of the weighted fine-tuning data as defined in Theorem 7.2), this direction is also the eigenvector of $\tilde{\boldsymbol{\Sigma}}'$ with the smallest eigenvalue.

Remark 7.5 (FLOW goes beyond model averaging). *If we perform model averaging between $\boldsymbol{\theta}_*$ and $\tilde{\boldsymbol{\theta}}_*$ with parameter $\omega \in [0, 1]$, then our averaged model is:*

$$\boldsymbol{\theta}_{\text{avg}}(\omega) = \omega \boldsymbol{\theta}_* + (1 - \omega) \tilde{\boldsymbol{\theta}}_* = \tilde{\boldsymbol{\theta}}_* + \omega \mathbf{e}. \quad (16)$$

Comparing the above with Eq. (15), we see that FLOW goes beyond model averaging because of the component along $\bar{\mathbf{e}}_\perp$. But we can make $\boldsymbol{\theta}_K$ (Eq. (15)) $\rightarrow \boldsymbol{\theta}_{\text{avg}}(\omega)$ by choosing $\beta \rightarrow 0$ and K such that $\gamma(K, \beta) \rightarrow \omega$. So, we expect **FLOW to be at least as powerful as model averaging**.

⁴The corresponding temperature is $\tau = \frac{2\beta(1-\rho^2)\|\mathbf{e}\|_2^2}{(1-\beta^2\rho^2)}$.

As per Lemma F.4, the minimum total error on both tasks with optimally tuned model averaging is given by:

$$\min_{\omega \in [0,1]} \text{err}_{\text{tot}}(\boldsymbol{\theta}_{\text{avg}}(\omega)) = \left(\frac{\bar{\mathbf{e}}^\top \boldsymbol{\Sigma} \bar{\mathbf{e}}}{\bar{\mathbf{e}}^\top \boldsymbol{\Sigma} \bar{\mathbf{e}} + 1} \right) \|\mathbf{e}\|_2^2 < \|\mathbf{e}\|_2^2, \quad (17)$$

where recall that $\boldsymbol{\Sigma}$ is the covariance matrix of the pre-training data. On the other hand, using Eqs. (5) and (13)

$$\min\left(\text{err}_{\text{tot}}(\boldsymbol{\theta}_*), \text{err}_{\text{tot}}(\tilde{\boldsymbol{\theta}}_*)\right) = \|\mathbf{e}\|_2^2. \quad (18)$$

Remark 7.6 (Error comparison). *By comparing Eqs. (17) and (18), we see that optimally tuned model averaging attains a smaller total error than both $\boldsymbol{\theta}_*$ (i.e., the pre-trained model) and $\tilde{\boldsymbol{\theta}}_*$ to which vanilla FT converges rapidly (Remark 7.3). More importantly, following our discussion in Remark 7.5, we conclude that **optimally tuned FLOW’s total error is at least as good as the one in Eq. (17).***

8 Conclusion

In this paper, we studied the problem of catastrophic forgetting in pre-trained models during fine-tuning when we do not have access to the pre-training data. To mitigate this issue, we proposed FLOW, a method which upweights easy samples based on the pre-trained loss values. Empirically, we showed that FLOW, on average, outperforms relevant baselines and is also complementary to these baselines in both vision and language settings. We also theoretically analyzed FLOW for linear models.

Acknowledgments

Ali Kavis is funded in part by the Swiss National Science Foundation (SNSF) under grant number P500PT_217942.

References

- Alec Radford, Jong Wook Kim, Chris Hallacy, Aditya Ramesh, Gabriel Goh, Sandhini Agarwal, Girish Sastry, Amanda Askell, Pamela Mishkin, Jack Clark, Gretchen Krueger, and Ilya Sutskever. Learning transferable visual models from natural language supervision. In Marina Meila and Tong Zhang, editors, *Proceedings of the 38th International Conference on Machine Learning*, volume 139 of *Proceedings of Machine Learning Research*, pages 8748–8763. PMLR, 18–24 Jul 2021. URL <https://proceedings.mlr.press/v139/radford21a.html>.
- Hugo Touvron, Thibaut Lavril, Gautier Izacard, Xavier Martinet, Marie-Anne Lachaux, Timothée Lacroix, Baptiste Rozière, Naman Goyal, Eric Hambro, Faisal Azhar, Aurelien Rodriguez, Armand Joulin, Edouard Grave, and Guillaume Lample. Llama: Open and efficient foundation language models, 2023a. URL <https://arxiv.org/abs/2302.13971>.
- Hugo Touvron, Louis Martin, Kevin R. Stone, Peter Albert, Amjad Almahairi, Yasmine Babaei, Nikolay Bashlykov, Soumya Batra, Prajjwal Bhargava, Shruti Bhosale, Daniel M. Bikel, Lukas Blecher, Cristian Cantón Ferrer, Moya Chen, Guillem Cucurull, David Esiobu, Jude Fernandes, Jeremy Fu, Wenyin Fu, Brian Fuller, Cynthia Gao, Vedanuj Goswami, Naman Goyal, Anthony S. Hartshorn, Saghar Hosseini, Rui Hou, Hakan Inan, Marcin Kardas, Viktor Kerkez, Madian Khabsa, Isabel M. Kloumann, A. V. Korenev, Punit Singh Koura, Marie-Anne Lachaux, Thibaut Lavril, Jenya Lee, Diana Liskovich, Yinghai Lu, Yuning Mao, Xavier Martinet, Todor Mihaylov, Pushkar Mishra, Igor Molybog, Yixin Nie, Andrew Poulton, Jeremy Reizenstein, Rashi Rungta, Kalyan Saladi, Alan Schelten, Ruan Silva, Eric Michael Smith, R. Subramanian, Xia Tan, Binh Tang, Ross Taylor, Adina Williams, Jian Xiang Kuan, Puxin Xu, Zhengxu Yan, Iliyan Zarov, Yuchen Zhang, Angela Fan, Melissa Hall Melanie Kambadur, Sharan Narang, Aurélien Rodriguez, Robert Stojnic, Sergey Edunov, and Thomas Scialom. Llama 2: Open foundation and fine-tuned chat models. *ArXiv*, abs/2307.09288, 2023b. URL <https://api.semanticscholar.org/CorpusID:259950998>.
- Aaron Grattafiori, Abhimanyu Dubey, Abhinav Jauhri, Abhinav Pandey, Abhishek Kadian, Ahmad Al-Dahle, Aiesha Letman, Akhil Mathur, Alan Schelten, Alex Vaughan, Amy Yang, Angela Fan, Anirudh Goyal, Anthony Hartshorn, Aobo Yang, Archi Mitra, Archie Sravankumar, Artem Korenev, Arthur Hinsvark, Arun Rao, Aston Zhang, Aurelien Rodriguez, Austen Gregerson, Ava Spataru, Baptiste Roziere, Bethany Biron, Binh Tang, Bobbie Chern, Charlotte Caucheteux, Chaya Nayak, Chloe Bi, Chris Marra, Chris McConnell, Christian Keller, Christophe Touret, Chunyang Wu, Corinne Wong, Cristian Canton Ferrer, Cyrus Nikolaidis, Damien Allonsius, Daniel Song, Danielle Pintz, Danny Livshits, Danny Wyatt, David Esiobu, Dhruv Choudhary, Dhruv Mahajan, Diego Garcia-Olano, Diego Perino, Dieuwke Hupkes, Egor Lakomkin, Ehab AlBadawy, Elina Lobanova, Emily Dinan, Eric Michael Smith, Filip Radenovic, Francisco Guzmán, Frank Zhang, Gabriel Synnaeve, Gabrielle Lee, Georgia Lewis Anderson, Govind Thattai, Graeme Nail, Gregoire Mialon, Guan Pang, Guillem Cucurell, Hailey Nguyen, Hannah Korevaar, Hu Xu, Hugo Touvron, Iliyan Zarov, Imanol Arrieta Ibarra, Isabel Kloumann, Ishan Misra, Ivan Evtimov, Jack Zhang, Jade Copet, Jaewon Lee, Jan Geffert, Jana Vranes, Jason Park, Jay Mahadeokar, Jeet Shah, Jelmer van der Linde, Jennifer Billock, Jenny Hong, Jenya Lee, Jeremy Fu, Jianfeng Chi, Jianyu Huang, Jiawen Liu, Jie Wang, Jiecao Yu, Joanna Bitton, Joe Spisak, Jongsoo Park, Joseph Rocca, Joshua Johnstun, Joshua Saxe, Junteng Jia, Kalyan Vasuden Alwala, Karthik Prasad, Kartikeya Upasani, Kate Plawiak, Ke Li, Kenneth Heafield, Kevin Stone, Khalid El-Arini, Krithika Iyer, Kshitiz Malik, Kuenley Chiu, Kunal Bhalla, Kushal Lakhotia, Lauren Rantala-Yearly, Laurens van der Maaten, Lawrence Chen, Liang Tan, Liz Jenkins, Louis Martin, Lovish Madaan, Lubo Malo, Lukas Blecher, Lukas Landzaat, Luke de Oliveira, Madeline Muzzi, Mahesh Pasupuleti,

Mannat Singh, Manohar Paluri, Marcin Kardas, Maria Tsimpoukelli, Mathew Oldham, Mathieu Rita, Maya Pavlova, Melanie Kambadur, Mike Lewis, Min Si, Mitesh Kumar Singh, Mona Hassan, Naman Goyal, Narjes Torabi, Nikolay Bashlykov, Nikolay Bogoychev, Niladri Chatterji, Ning Zhang, Olivier Duchenne, Onur Çelebi, Patrick Alrassy, Pengchuan Zhang, Pengwei Li, Petar Vasic, Peter Weng, Prajjwal Bhargava, Pratik Dubal, Praveen Krishnan, Punit Singh Koura, Puxin Xu, Qing He, Qingxiao Dong, Ragavan Srinivasan, Raj Ganapathy, Ramon Calderer, Ricardo Silveira Cabral, Robert Stojnic, Roberta Raileanu, Rohan Maheswari, Rohit Girdhar, Rohit Patel, Romain Sauvestre, Ronnie Polidoro, Roshan Sumbaly, Ross Taylor, Ruan Silva, Rui Hou, Rui Wang, Saghar Hosseini, Sahana Chennabasappa, Sanjay Singh, Sean Bell, Seohyun Sonia Kim, Sergey Edunov, Shaoliang Nie, Sharan Narang, Sharath Raparthy, Sheng Shen, Shengye Wan, Shruti Bhosale, Shun Zhang, Simon Vandenhende, Soumya Batra, Spencer Whitman, Sten Sootla, Stephane Collot, Suchin Gururangan, Sydney Borodinsky, Tamar Herman, Tara Fowler, Tarek Sheasha, Thomas Georgiou, Thomas Scialom, Tobias Speckbacher, Todor Mihaylov, Tong Xiao, Ujjwal Karn, Vedanuj Goswami, Vibhor Gupta, Vignesh Ramanathan, Viktor Kerkez, Vincent Conguet, Virginie Do, Vish Vogeti, Vitor Albiero, Vladan Petrovic, Weiwei Chu, Wenhan Xiong, Wenyan Fu, Whitney Meers, Xavier Martinet, Xiaodong Wang, Xiaofang Wang, Xiaoqing Ellen Tan, Xide Xia, Xinfeng Xie, Xuchao Jia, Xuwei Wang, Yaelle Goldschlag, Yashesh Gaur, Yasmine Babaei, Yi Wen, Yiwen Song, Yuchen Zhang, Yue Li, Yuning Mao, Zacharie Delpierre Coudert, Zheng Yan, Zhengxing Chen, Zoe Papanikos, Aaditya Singh, Aayushi Srivastava, Abha Jain, Adam Kelsey, Adam Shajnfeld, Adithya Gangidi, Adolfo Victoria, Ahuva Goldstand, Ajay Menon, Ajay Sharma, Alex Boesenberg, Alexei Baevski, Allie Feinstein, Amanda Kallet, Amit Sangani, Amos Teo, Anam Yunus, Andrei Lupu, Andres Alvarado, Andrew Caples, Andrew Gu, Andrew Ho, Andrew Poulton, Andrew Ryan, Ankit Ramchandani, Annie Dong, Annie Franco, Anuj Goyal, Aparajita Saraf, Arkabandhu Chowdhury, Ashley Gabriel, Ashwin Bharambe, Assaf Eisenman, Azadeh Yazdan, Beau James, Ben Maurer, Benjamin Leonhardi, Bernie Huang, Beth Loyd, Beto De Paola, Bhargavi Paranjape, Bing Liu, Bo Wu, Boyu Ni, Braden Hancock, Bram Wasti, Brandon Spence, Brani Stojkovic, Brian Gamido, Britt Montalvo, Carl Parker, Carly Burton, Catalina Mejia, Ce Liu, Changhan Wang, Changkyu Kim, Chao Zhou, Chester Hu, Ching-Hsiang Chu, Chris Cai, Chris Tindal, Christoph Feichtenhofer, Cynthia Gao, Damon Civin, Dana Beaty, Daniel Kreymer, Daniel Li, David Adkins, David Xu, Davide Testuggine, Delia David, Devi Parikh, Diana Liskovich, Didem Foss, Dingkan Wang, Duc Le, Dustin Holland, Edward Dowling, Eissa Jamil, Elaine Montgomery, Eleonora Presani, Emily Hahn, Emily Wood, Eric-Tuan Le, Erik Brinkman, Esteban Arcaute, Evan Dunbar, Evan Smothers, Fei Sun, Felix Kreuk, Feng Tian, Filippos Kokkinos, Firat Ozgenel, Francesco Caggioni, Frank Kanayet, Frank Seide, Gabriela Medina Florez, Gabriella Schwarz, Gada Badeer, Georgia Swee, Gil Halpern, Grant Herman, Grigory Sizov, Guangyi, Zhang, Guna Lakshminarayanan, Hakan Inan, Hamid Shojanazeri, Han Zou, Hannah Wang, Hanwen Zha, Haroun Habeeb, Harrison Rudolph, Helen Suk, Henry Aspegren, Hunter Goldman, Hongyuan Zhan, Ibrahim Damla, Igor Molybog, Igor Tufanov, Ilias Leontiadis, Irina-Elena Veliche, Itai Gat, Jake Weissman, James Geboski, James Kohli, Janice Lam, Japhet Asher, Jean-Baptiste Gaya, Jeff Marcus, Jeff Tang, Jennifer Chan, Jenny Zhen, Jeremy Reizenstein, Jeremy Teboul, Jessica Zhong, Jian Jin, Jingyi Yang, Joe Cummings, Jon Carvill, Jon Shepard, Jonathan McPhie, Jonathan Torres, Josh Ginsburg, Junjie Wang, Kai Wu, Kam Hou U, Karan Saxena, Kartikay Khandelwal, Katayoun Zand, Kathy Matosich, Kaushik Veeraraghavan, Kelly Michelen, Keqian Li, Kiran Jagadeesh, Kun Huang, Kunal Chawla, Kyle Huang, Lailin Chen, Lakshya Garg, Lavender A, Leandro Silva, Lee Bell, Lei Zhang, Liangpeng Guo, Licheng Yu, Liron Moshkovich, Luca Wehrstedt, Madian Khabsa, Manav Avalani, Manish Bhatt, Martynas Mankus, Matan Hasson, Matthew Lennie, Matthias Reso, Maxim Groshev, Maxim Naumov, Maya Lathi, Meghan Keneally, Miao Liu, Michael L. Seltzer, Michal Valko, Michelle Restrepo, Mihir

- Patel, Mik Vyatskov, Mikayel Samvelyan, Mike Clark, Mike Macey, Mike Wang, Miquel Jubert Hermoso, Mo Metanat, Mohammad Rastegari, Munish Bansal, Nandhini Santhanam, Natascha Parks, Natasha White, Navyata Bawa, Nayan Singhal, Nick Egebo, Nicolas Usunier, Nikhil Mehta, Nikolay Pavlovich Laptev, Ning Dong, Norman Cheng, Oleg Chernoguz, Olivia Hart, Omkar Salpekar, Ozlem Kalinli, Parkin Kent, Parth Parekh, Paul Saab, Pavan Balaji, Pedro Rittner, Philip Bontrager, Pierre Roux, Piotr Dollar, Polina Zvyagina, Prashant Ratanchandani, Pritish Yuvraj, Qian Liang, Rachad Alao, Rachel Rodriguez, Rafi Ayub, Raghotham Murthy, Raghu Nayani, Rahul Mitra, Rangaprabhu Parthasarathy, Raymond Li, Rebekkah Hogan, Robin Battey, Rocky Wang, Russ Howes, Ruty Rinott, Sachin Mehta, Sachin Siby, Sai Jayesh Bondu, Samyak Datta, Sara Chugh, Sara Hunt, Sargun Dhillon, Sasha Sidorov, Satadru Pan, Saurabh Mahajan, Saurabh Verma, Seiji Yamamoto, Sharadh Ramaswamy, Shaun Lindsay, Sheng Feng, Shenghao Lin, Shengxin Cindy Zha, Shishir Patil, Shiva Shankar, Shuqiang Zhang, Shuqiang Zhang, Sinong Wang, Sneha Agarwal, Soji Sajuyigbe, Soumith Chintala, Stephanie Max, Stephen Chen, Steve Kehoe, Steve Satterfield, Sudarshan Govindaprasad, Sumit Gupta, Summer Deng, Sungmin Cho, Sunny Virk, Suraj Subramanian, Sy Choudhury, Sydney Goldman, Tal Remez, Tamar Glaser, Tamara Best, Thilo Koehler, Thomas Robinson, Tianhe Li, Tianjun Zhang, Tim Matthews, Timothy Chou, Tzook Shaked, Varun Vontimitta, Victoria Ajayi, Victoria Montanez, Vijai Mohan, Vinay Satish Kumar, Vishal Mangla, Vlad Ionescu, Vlad Poenaru, Vlad Tiberiu Mihailescu, Vladimir Ivanov, Wei Li, Wenchen Wang, Wenwen Jiang, Wes Bouaziz, Will Constable, Xiaocheng Tang, Xiaojian Wu, Xiaolan Wang, Xilun Wu, Xinbo Gao, Yaniv Kleinman, Yanjun Chen, Ye Hu, Ye Jia, Ye Qi, Yenda Li, Yilin Zhang, Ying Zhang, Yossi Adi, Youngjin Nam, Yu, Wang, Yu Zhao, Yuchen Hao, Yundi Qian, Yunlu Li, Yuzi He, Zach Rait, Zachary DeVito, Zef Rosnbrick, Zhaoduo Wen, Zhenyu Yang, Zhiwei Zhao, and Zhiyu Ma. The llama 3 herd of models, 2024. URL <https://arxiv.org/abs/2407.21783>.
- Albert Q. Jiang, Alexandre Sablayrolles, Arthur Mensch, Chris Bamford, Devendra Singh Chaplot, Diego de Las Casas, Florian Bressand, Gianna Lengyel, Guillaume Lample, Lucile Saulnier, L elio Renard Lavaud, Marie-Anne Lachaux, Pierre Stock, Teven Le Scao, Thibaut Lavril, Thomas Wang, Timoth e Lacroix, and William El Sayed. Mistral 7b. *CoRR*, abs/2310.06825, 2023. doi:10.48550/ARXIV.2310.06825. URL <https://doi.org/10.48550/arXiv.2310.06825>.
- Ilya Loshchilov and Frank Hutter. Online batch selection for faster training of neural networks. *ArXiv*, abs/1511.06343, 2015. URL <https://api.semanticscholar.org/CorpusID:5324823>.
- Abhinav Shrivastava, Abhinav Gupta, and Ross Girshick. Training region-based object detectors with online hard example mining. In *2016 IEEE Conference on Computer Vision and Pattern Recognition (CVPR)*, pages 761–769, 2016. doi:10.1109/CVPR.2016.89.
- Angelos Katharopoulos and Fran ois Fleuret. Biased importance sampling for deep neural network training. *arXiv preprint arXiv:1706.00043*, 2017.
- Kenji Kawaguchi and Haihao Lu. Ordered sgd: A new stochastic optimization framework for empirical risk minimization. In *International Conference on Artificial Intelligence and Statistics*, pages 669–679. PMLR, 2020.
- Rudrajit Das, Xi Chen, Bertram Ieong, Parikshit Bansal, et al. Understanding the training speedup from sampling with approximate losses. In *Forty-first International Conference on Machine Learning*, 2024.
- Hongjoon Ahn, Sungmin Cha, Donggyu Lee, and Taesup Moon. Uncertainty-based continual learning with adaptive regularization. In H. Wallach, H. Larochelle, A. Beygelzimer, F. d'Alch e-Buc,

- E. Fox, and R. Garnett, editors, *Advances in Neural Information Processing Systems*, volume 32. Curran Associates, Inc., 2019. URL https://proceedings.neurips.cc/paper_files/paper/2019/file/2c3ddf4bf13852db711dd1901fb517fa-Paper.pdf.
- James Kirkpatrick, Razvan Pascanu, Neil C. Rabinowitz, Joel Veness, Guillaume Desjardins, Andrei A. Rusu, Kieran Milan, John Quan, Tiago Ramalho, Agnieszka Grabska-Barwinska, Demis Hassabis, Claudia Clopath, Dharshan Kumaran, and Raia Hadsell. Overcoming catastrophic forgetting in neural networks. *Proceedings of the National Academy of Sciences*, 114:3521 – 3526, 2016. URL <https://api.semanticscholar.org/CorpusID:4704285>.
- Jonathan Schwarz, Wojciech Czarnecki, Jelena Luketina, Agnieszka Grabska-Barwinska, Yee Whye Teh, Razvan Pascanu, and Raia Hadsell. Progress & compress: A scalable framework for continual learning. In Jennifer Dy and Andreas Krause, editors, *Proceedings of the 35th International Conference on Machine Learning*, volume 80 of *Proceedings of Machine Learning Research*, pages 4528–4537. PMLR, 10–15 Jul 2018. URL <https://proceedings.mlr.press/v80/schwarz18a.html>.
- Hippolyt Ritter, Aleksandar Botev, and David Barber. Online structured laplace approximations for overcoming catastrophic forgetting. In *Proceedings of the 32nd International Conference on Neural Information Processing Systems*, NIPS’18, page 3742–3752, Red Hook, NY, USA, 2018. Curran Associates Inc.
- Janghyeon Lee, Hyeong Gwon Hong, Donggyu Joo, and Junmo Kim. Continual learning with extended kronecker-factored approximate curvature. *2020 IEEE/CVF Conference on Computer Vision and Pattern Recognition (CVPR)*, pages 8998–9007, 2020. URL <https://api.semanticscholar.org/CorpusID:215786151>.
- Xialei Liu, Marc Masana, Luis Herranz, Joost Van de Weijer, Antonio M. López, and Andrew D. Bagdanov. Rotate your networks: Better weight consolidation and less catastrophic forgetting. In *2018 24th International Conference on Pattern Recognition (ICPR)*, pages 2262–2268, 2018. doi:10.1109/ICPR.2018.8545895.
- Friedemann Zenke, Ben Poole, and Surya Ganguli. Continual learning through synaptic intelligence. In Doina Precup and Yee Whye Teh, editors, *Proceedings of the 34th International Conference on Machine Learning*, volume 70 of *Proceedings of Machine Learning Research*, pages 3987–3995. PMLR, 06–11 Aug 2017. URL <https://proceedings.mlr.press/v70/zenke17a.html>.
- Rahaf Aljundi, Francesca Babiloni, Mohamed Elhoseiny, Marcus Rohrbach, and Tinne Tuytelaars. Memory aware synapses: Learning what (not) to forget. In *Computer Vision – ECCV 2018: 15th European Conference, Munich, Germany, September 8–14, 2018, Proceedings, Part III*, page 144–161, Berlin, Heidelberg, 2018. Springer-Verlag. ISBN 978-3-030-01218-2. doi:10.1007/978-3-030-01219-9_9. URL https://doi.org/10.1007/978-3-030-01219-9_9.
- Sang-Woo Lee, Jin-Hwa Kim, Jaehyun Jun, Jung-Woo Ha, and Byoung-Tak Zhang. Overcoming catastrophic forgetting by incremental moment matching. In *Proceedings of the 31st International Conference on Neural Information Processing Systems*, NIPS’17, page 4655–4665, Red Hook, NY, USA, 2017. Curran Associates Inc. ISBN 9781510860964.
- David Lopez-Paz and Marc’Aurelio Ranzato. Gradient episodic memory for continual learning. In *Proceedings of the 31st International Conference on Neural Information Processing Systems*, NIPS’17, page 6470–6479, Red Hook, NY, USA, 2017. Curran Associates Inc. ISBN 9781510860964.

- Mehrdad Farajtabar, Navid Azizan, Alex Mott, and Ang Li. Orthogonal gradient descent for continual learning. In Silvia Chiappa and Roberto Calandra, editors, *Proceedings of the Twenty Third International Conference on Artificial Intelligence and Statistics*, volume 108 of *Proceedings of Machine Learning Research*, pages 3762–3773. PMLR, 26–28 Aug 2020. URL <https://proceedings.mlr.press/v108/farajtabar20a.html>.
- Arslan Chaudhry, Marc’Aurelio Ranzato, Marcus Rohrbach, and Mohamed Elhoseiny. Efficient lifelong learning with a-GEM. In *International Conference on Learning Representations*, 2019a. URL https://openreview.net/forum?id=Hkf2_sC5FX.
- Guanxiong Zeng, Yang Chen, Bo Cui, and Shan Yu. Continual learning of context-dependent processing in neural networks. *Nature Machine Intelligence*, 1:364–372, 08 2019. doi:10.1038/s42256-019-0080-x.
- Shipeng Wang, Xiaorong Li, Jian Sun, and Zongben Xu. Training networks in null space of feature covariance for continual learning. pages 184–193, 06 2021. doi:10.1109/CVPR46437.2021.00025.
- Xiao Wang, Tianze Chen, Qiming Ge, Han Xia, Rong Bao, Rui Zheng, Qi Zhang, Tao Gui, and Xuanjing Huang. Orthogonal subspace learning for language model continual learning. In Houda Bouamor, Juan Pino, and Kalika Bali, editors, *Findings of the Association for Computational Linguistics: EMNLP 2023*, pages 10658–10671, Singapore, December 2023a. Association for Computational Linguistics. doi:10.18653/v1/2023.findings-emnlp.715. URL <https://aclanthology.org/2023.findings-emnlp.715/>.
- Sylvestre-Alvise Rebuffi, Alexander Kolesnikov, Georg Sperl, and Christoph H. Lampert. icarl: Incremental classifier and representation learning. In *2017 IEEE Conference on Computer Vision and Pattern Recognition (CVPR)*, pages 5533–5542, 2017. doi:10.1109/CVPR.2017.587.
- Rahaf Aljundi, Min Lin, Baptiste Goujaud, and Yoshua Bengio. *Gradient based sample selection for online continual learning*. Curran Associates Inc., Red Hook, NY, USA, 2019.
- Jihwan Bang, Heesu Kim, Young Joon Yoo, Jung-Woo Ha, and Jonghyun Choi. Rainbow memory: Continual learning with a memory of diverse samples. *2021 IEEE/CVF Conference on Computer Vision and Pattern Recognition (CVPR)*, pages 8214–8223, 2021. URL <https://api.semanticscholar.org/CorpusID:232427874>.
- A Chaudhry, M Rohrbach, M Elhoseiny, T Ajanthan, P Dokania, P Torr, and M Ranzato. Continual learning with tiny episodic memories. 2019b.
- David Isele and Akansel Cosgun. Selective experience replay for lifelong learning. In *Proceedings of the Thirty-Second AAAI Conference on Artificial Intelligence and Thirtieth Innovative Applications of Artificial Intelligence Conference and Eighth AAAI Symposium on Educational Advances in Artificial Intelligence*, AAAI’18/IAAI’18/EAAI’18. AAAI Press, 2018. ISBN 978-1-57735-800-8.
- Matthias De Lange and Tinne Tuytelaars. Continual prototype evolution: Learning online from non-stationary data streams. In *Proceedings of the IEEE/CVF International Conference on Computer Vision (ICCV)*, pages 8250–8259, October 2021.
- Zalán Borsos, Mojmir Mutny, and Andreas Krause. Coresets via bilevel optimization for continual learning and streaming. In H. Larochelle, M. Ranzato, R. Hadsell, M.F. Balcan, and H. Lin, editors, *Advances in Neural Information Processing Systems*, volume 33, pages 14879–14890. Curran Associates, Inc., 2020. URL https://proceedings.neurips.cc/paper_files/paper/2020/file/aa2a77371374094fe9e0bc1de3f94ed9-Paper.pdf.

- Rishabh Tiwari, Krishnateja Killamsetty, Rishabh Iyer, and Pradeep Shenoy. Gcr: Gradient coreset based replay buffer selection for continual learning. *CVPR*, 11 2021. doi:10.48550/arXiv.2111.11210.
- Daniel L. Silver and Robert E. Mercer. The task rehearsal method of life-long learning: Overcoming impoverished data. In *Proceedings of the 15th Conference of the Canadian Society for Computational Studies of Intelligence on Advances in Artificial Intelligence*, AI '02, page 90–101, Berlin, Heidelberg, 2002. Springer-Verlag. ISBN 354043724X.
- Zhizhong Li and Derek Hoiem. Learning without forgetting. In Bastian Leibe, Jiri Matas, Nicu Sebe, and Max Welling, editors, *ECCV (4)*, volume 9908 of *Lecture Notes in Computer Science*, pages 614–629. Springer, 2016. ISBN 978-3-319-46492-3. URL <http://dblp.uni-trier.de/db/conf/eccv/eccv2016-4.html#LiH16>.
- A. Triki, Rahaf Aljundi, Matthew B. Blaschko, and Tinne Tuytelaars. Encoder based lifelong learning. *2017 IEEE International Conference on Computer Vision (ICCV)*, pages 1329–1337, 2017. URL <https://api.semanticscholar.org/CorpusID:12253672>.
- Kibok Lee, Kimin Lee, Jinwoo Shin, and Honglak Lee. Overcoming catastrophic forgetting with unlabeled data in the wild. *2019 IEEE/CVF International Conference on Computer Vision (ICCV)*, pages 312–321, 2019a. URL <https://api.semanticscholar.org/CorpusID:201314887>.
- Prithviraj Dhar, Rajat Vikram Singh, Kuan-Chuan Peng, Ziyang Wu, and Rama Chellappa. Learning without memorizing. In *IEEE Conference on Computer Vision and Pattern Recognition, CVPR 2019, Long Beach, CA, USA, June 16-20, 2019*, pages 5138–5146. Computer Vision Foundation / IEEE, 2019. doi:10.1109/CVPR.2019.00528. URL http://openaccess.thecvf.com/content_CVPR_2019/html/Dhar_Learning_Without_Memorizing_CVPR_2019_paper.html.
- Matthew Riemer, Ignacio Cases, Robert Ajemian, Miao Liu, Irina Rish, Yuhai Tu, and Gerald Tesaro. Learning to learn without forgetting by maximizing transfer and minimizing interference. In *7th International Conference on Learning Representations, ICLR 2019, New Orleans, LA, USA, May 6-9, 2019*. OpenReview.net, 2019. URL <https://openreview.net/forum?id=B1gTShAct7>.
- Andrei A. Rusu, Neil C. Rabinowitz, Guillaume Desjardins, Hubert Soyer, James Kirkpatrick, Koray Kavukcuoglu, Razvan Pascanu, and Raia Hadsell. Progressive neural networks. *ArXiv*, abs/1606.04671, 2016. URL <https://api.semanticscholar.org/CorpusID:15350923>.
- Rahaf Aljundi, Punarjay Chakravarty, and Tinne Tuytelaars. Expert gate: Lifelong learning with a network of experts. In *2017 IEEE Conference on Computer Vision and Pattern Recognition (CVPR)*, pages 7120–7129, 2017. doi:10.1109/CVPR.2017.753.
- Mark Patrick Collier, Effrosyni Kokiopoulou, Andrea Gesmundo, and Jesse Berent. Routing networks with co-training for continual learning. In *ICML 2020 Workshop on Continual Learning*, 2020.
- Jathushan Rajasegaran, Munawar Hayat, Salman Khan, Fahad Shahbaz Khan, and Ling Shao. *Random path selection for incremental learning*. Curran Associates Inc., Red Hook, NY, USA, 2019.
- Rahul Ramesh and Pratik Chaudhari. Model zoo: A growing brain that learns continually. In *International Conference on Learning Representations*, 2021. URL <https://api.semanticscholar.org/CorpusID:245007201>.

- Liyuan Wang, Xingxing Zhang, Qian Li, Mingtian Zhang, Hang Su, Jun Zhu, and Yi Zhong. Incorporating neuro-inspired adaptability for continual learning in artificial intelligence. *Nature Machine Intelligence*, 5:1–13, 11 2023b. doi:10.1038/s42256-023-00747-w.
- Liyuan Wang, Xingxing Zhang, Qian Li, Jun Zhu, and Yi Zhong. Coscl: Cooperation of small continual learners is stronger than a big one. In *Computer Vision – ECCV 2022: 17th European Conference, Tel Aviv, Israel, October 23–27, 2022, Proceedings, Part XXVI*, page 254–271, Berlin, Heidelberg, 2022a. Springer-Verlag. ISBN 978-3-031-19808-3. doi:10.1007/978-3-031-19809-0_15. URL https://doi.org/10.1007/978-3-031-19809-0_15.
- Jaehong Yoon, Eunho Yang, Jeongtae Lee, and Sung Ju Hwang. Lifelong learning with dynamically expandable networks. In *International Conference on Learning Representations*, 2018. URL <https://openreview.net/forum?id=Sk7KsfW0->.
- Oleksiy Ostapenko, Mihai Marian Puscas, Tassilo Klein, Patrick Jähnichen, and Moin Nabi. Learning to remember: A synaptic plasticity driven framework for continual learning. *2019 IEEE/CVF Conference on Computer Vision and Pattern Recognition (CVPR)*, pages 11313–11321, 2019. URL <https://api.semanticscholar.org/CorpusID:102353035>.
- Steven C. Y. Hung, Cheng-Hao Tu, Cheng-En Wu, Chien-Hung Chen, Yi-Ming Chan, and Chu-Song Chen. *Compacting, picking and growing for unforgetting continual learning*. Curran Associates Inc., Red Hook, NY, USA, 2019.
- Arun Mallya, Dillon Davis, and Svetlana Lazebnik. Piggyback: Adapting a single network to multiple tasks by learning to mask weights. In *Computer Vision – ECCV 2018: 15th European Conference, Munich, Germany, September 8–14, 2018, Proceedings, Part IV*, page 72–88, Berlin, Heidelberg, 2018. Springer-Verlag. ISBN 978-3-030-01224-3. doi:10.1007/978-3-030-01225-0_5. URL https://doi.org/10.1007/978-3-030-01225-0_5.
- Haeyong Kang, Rusty John Lloyd Mina, Sultan Rizky Hikmawan Madjid, Jaehong Yoon, Mark Hasegawa-Johnson, Sung Ju Hwang, and Chang D. Yoo. Forget-free continual learning with winning subnetworks. In Kamalika Chaudhuri, Stefanie Jegelka, Le Song, Csaba Szepesvari, Gang Niu, and Sivan Sabato, editors, *Proceedings of the 39th International Conference on Machine Learning*, volume 162 of *Proceedings of Machine Learning Research*, pages 10734–10750. PMLR, 17–23 Jul 2022. URL <https://proceedings.mlr.press/v162/kang22b.html>.
- Joan Serra, Didac Suris, Marius Miron, and Alexandros Karatzoglou. Overcoming catastrophic forgetting with hard attention to the task. In Jennifer Dy and Andreas Krause, editors, *Proceedings of the 35th International Conference on Machine Learning*, volume 80 of *Proceedings of Machine Learning Research*, pages 4548–4557. PMLR, 10–15 Jul 2018. URL <https://proceedings.mlr.press/v80/serra18a.html>.
- Mitchell Wortsman, Vivek Ramanujan, Rosanne Liu, Aniruddha Kembhavi, Mohammad Rastegari, Jason Yosinski, and Ali Farhadi. Supermasks in superposition. In *Proceedings of the 34th International Conference on Neural Information Processing Systems, NIPS ’20*, Red Hook, NY, USA, 2020. Curran Associates Inc. ISBN 9781713829546.
- Arun Mallya and Svetlana Lazebnik. Packnet: Adding multiple tasks to a single network by iterative pruning. *2018 IEEE/CVF Conference on Computer Vision and Pattern Recognition*, pages 7765–7773, 2017. URL <https://api.semanticscholar.org/CorpusID:35249701>.

- Constantine Dvornik, Mustafa B Gurbuz. Nispa: Neuro-inspired stability-plasticity adaptation for continual learning in sparse networks. *Proceedings of the 39th International Conference on Machine Learning*, 162, 2022. URL <https://par.nsf.gov/biblio/10389701>.
- Sangwon Jung, Hongjoon Ahn, Sungmin Cha, and Taesup Moon. Continual learning with node-importance based adaptive group sparse regularization. In *Proceedings of the 34th International Conference on Neural Information Processing Systems*, NIPS '20, Red Hook, NY, USA, 2020. Curran Associates Inc. ISBN 9781713829546.
- Ekdeep Singh Lubana, Puja Trivedi, Danai Koutra, and R. Dick. How do quadratic regularizers prevent catastrophic forgetting: The role of interpolation. *COLLAS*, 2021.
- Mitchell Wortsman, Gabriel Ilharco, Jong Wook Kim, Mike Li, Simon Kornblith, Rebecca Roelofs, Raphael Gontijo-Lopes, Hannaneh Hajishirzi, Ali Farhadi, Hongseok Namkoong, and Ludwig Schmidt. Robust fine-tuning of zero-shot models. *arXiv preprint arXiv:2109.01903*, 2021. <https://arxiv.org/abs/2109.01903>.
- Gabriel Ilharco, Marco Tulio Ribeiro, Mitchell Wortsman, Ludwig Schmidt, Hannaneh Hajishirzi, and Ali Farhadi. Editing models with task arithmetic. In *The Eleventh International Conference on Learning Representations*, 2023. URL <https://openreview.net/forum?id=6t0Kwf8-jrj>.
- Yong Lin, Hangyu Lin, Wei Xiong, Shizhe Diao, Jianmeng Liu, Jipeng Zhang, Rui Pan, Haoxiang Wang, Wenbin Hu, Hanning Zhang, et al. Mitigating the alignment tax of rlhf. *CoRR*, 2023.
- Anat Kleiman, Gintare Karolina Dziugaite, Jonathan Frankle, Sham Kakade, and Mansheej Paul. Soup to go: mitigating forgetting during continual learning with model averaging, 2025. URL <https://arxiv.org/abs/2501.05559>.
- Yupeng Chen, Senmiao Wang, Zhihang Lin, Zeyu Qin, Yushun Zhang, Tian Ding, and Ruoyu Sun. Mofo: Momentum-filtered optimizer for mitigating forgetting in llm fine-tuning. *arXiv preprint arXiv:2407.20999*, 2024a.
- Ashwinee Panda, Berivan Isik, Xiangyu Qi, Sanmi Koyejo, Tsachy Weissman, and Prateek Mittal. Lottery ticket adaptation: Mitigating destructive interference in llms, 2024. <https://arxiv.org/abs/2406.16797>, 2024.
- Dan Biderman, Jacob Portes, Jose Javier Gonzalez Ortiz, Mansheej Paul, Philip Greengard, Connor Jennings, Daniel King, Sam Havens, Vitaliy Chiley, Jonathan Frankle, Cody Blakeney, and John Patrick Cunningham. LoRA learns less and forgets less. *Transactions on Machine Learning Research*, 2024. ISSN 2835-8856. URL <https://openreview.net/forum?id=aloEru2qCG>. Featured Certification.
- Edward J Hu, Yelong Shen, Phillip Wallis, Zeyuan Allen-Zhu, Yuanzhi Li, Shean Wang, Lu Wang, and Weizhu Chen. LoRA: Low-rank adaptation of large language models. In *International Conference on Learning Representations*, 2022. URL <https://openreview.net/forum?id=nZeVKeeFYf9>.
- Deanna Needell, Nathan Srebro, and Rachel Ward. Stochastic gradient descent, weighted sampling, and the randomized kaczmarz algorithm. In *Proceedings of the 28th International Conference on Neural Information Processing Systems - Volume 1*, NIPS'14, page 1017–1025, Cambridge, MA, USA, 2014. MIT Press.

- Peilin Zhao and Tong Zhang. Stochastic optimization with importance sampling for regularized loss minimization. In *Proceedings of the 32nd International Conference on International Conference on Machine Learning - Volume 37*, ICML'15, page 1–9. JMLR.org, 2015.
- Guillaume Alain, Alex Lamb, Chinnadhurai Sankar, Aaron C. Courville, and Yoshua Bengio. Variance reduction in sgd by distributed importance sampling. *ArXiv*, abs/1511.06481, 2015. URL <https://api.semanticscholar.org/CorpusID:6546520>.
- Sebastian U. Stich, Anant Raj, and Martin Jaggi. Safe adaptive importance sampling. In *Proceedings of the 31st International Conference on Neural Information Processing Systems*, NIPS'17, page 4384–4394, Red Hook, NY, USA, 2017. Curran Associates Inc. ISBN 9781510860964.
- Angelos Katharopoulos and Francois Fleuret. Not all samples are created equal: Deep learning with importance sampling. In Jennifer Dy and Andreas Krause, editors, *Proceedings of the 35th International Conference on Machine Learning*, volume 80 of *Proceedings of Machine Learning Research*, pages 2525–2534. PMLR, 10–15 Jul 2018. URL <https://proceedings.mlr.press/v80/katharopoulos18a.html>.
- Aharon Ben-Tal, Dick Den Hertog, Anja De Waegenaere, Bertrand Melenberg, and Gijs Rennen. Robust solutions of optimization problems affected by uncertain probabilities. *Management Science*, 59(2):341–357, 2013.
- Daniel Levy, Yair Carmon, John C Duchi, and Aaron Sidford. Large-scale methods for distributionally robust optimization. *Advances in Neural Information Processing Systems*, 33:8847–8860, 2020.
- John C Duchi and Hongseok Namkoong. Learning models with uniform performance via distributionally robust optimization. *The Annals of Statistics*, 49(3):1378–1406, 2021.
- Qi Qi, Zhishuai Guo, Yi Xu, Rong Jin, and Tianbao Yang. An online method for a class of distributionally robust optimization with non-convex objectives. *Advances in Neural Information Processing Systems*, 34:10067–10080, 2021.
- Sang Michael Xie, Hieu Pham, Xuanyi Dong, Nan Du, Hanxiao Liu, Yifeng Lu, Percy S Liang, Quoc V Le, Tengyu Ma, and Adams Wei Yu. Doremi: Optimizing data mixtures speeds up language model pretraining. *Advances in Neural Information Processing Systems*, 36, 2024.
- Xuxi Chen, Zhendong Wang, Daouda Sow, Junjie Yang, Tianlong Chen, Yingbin Liang, Mingyuan Zhou, and Zhangyang Wang. Take the bull by the horns: Hard sample-reweighted continual training improves llm generalization. *arXiv preprint arXiv:2402.14270*, 2024b.
- Anonymous. Dynamic loss-based sample reweighting for improved large language model pretraining. In *The Thirteenth International Conference on Learning Representations*, 2025. URL <https://openreview.net/forum?id=gU4ZgQNs0C>.
- Olga Russakovsky, Jia Deng, Hao Su, Jonathan Krause, Sanjeev Satheesh, Sean Ma, Zhiheng Huang, Andrej Karpathy, Aditya Khosla, Michael Bernstein, et al. Imagenet large scale visual recognition challenge. *International journal of computer vision*, 115:211–252, 2015.
- Ross Wightman, Hugo Touvron, and Hervé Jégou. Resnet strikes back: An improved training procedure in timm. *NEURIPS*, workshop.
- Alex Krizhevsky. Learning multiple layers of features from tiny images. Technical report, 2009.

- Maria-Elena Nilsback and Andrew Zisserman. Automated flower classification over a large number of classes. In *2008 Sixth Indian Conference on Computer Vision, Graphics & Image Processing*, pages 722–729, 2008. doi:10.1109/ICVGIP.2008.47.
- Fei-Fei Li, Marco Andreeto, Marc’Aurelio Ranzato, and Pietro Perona. Caltech 101, Apr 2022.
- Jonathan Krause, Michael Stark, Jia Deng, and Li Fei-Fei. 3d object representations for fine-grained categorization. In *2013 IEEE International Conference on Computer Vision Workshops*, pages 554–561, 2013. doi:10.1109/ICCVW.2013.77.
- Omkar M Parkhi, Andrea Vedaldi, and Andrew Zisserman. Dogs: A dataset for recognising dog breeds from images. In *British Machine Vision Conference (BMVC)*, 2012.
- Sachin Goyal, Ananya Kumar, Sankalp Garg, Zico Kolter, and Aditi Raghunathan. Finetune like you pretrain: Improved finetuning of zero-shot vision models. *CVPR*, 2023.
- Sourab Mangrulkar, Sylvain Gugger, Lysandre Debut, Younes Belkada, Sayak Paul, and Benjamin Bossan. Peft: State-of-the-art parameter-efficient fine-tuning methods. <https://github.com/huggingface/peft>, 2022.
- Thomas Wolf, Lysandre Debut, Victor Sanh, Julien Chaumond, Clement Delangue, Anthony Moi, Pierric Cistac, Tim Rault, Rémi Louf, Morgan Funtowicz, Joe Davison, Sam Shleifer, Patrick von Platen, Clara Ma, Yacine Jernite, Julien Plu, Canwen Xu, Teven Le Scao, Sylvain Gugger, Mariama Drame, Quentin Lhoest, and Alexander M. Rush. Transformers: State-of-the-art natural language processing. In *Proceedings of the 2020 Conference on Empirical Methods in Natural Language Processing: System Demonstrations*, pages 38–45, Online, October 2020. Association for Computational Linguistics. URL <https://www.aclweb.org/anthology/2020.emnlp-demos.6>.
- Quentin Lhoest, Albert Villanova del Moral, Yacine Jernite, Abhishek Thakur, Patrick von Platen, Suraj Patil, Julien Chaumond, Mariama Drame, Julien Plu, Lewis Tunstall, Joe Davison, Mario Šaško, Gunjan Chhablani, Bhavitvya Malik, Simon Brandeis, Teven Le Scao, Victor Sanh, Canwen Xu, Nicolas Patry, Angelina McMillan-Major, Philipp Schmid, Sylvain Gugger, Clément Delangue, Théo Matussière, Lysandre Debut, Stas Bekman, Pierric Cistac, Thibault Goehringer, Victor Mustar, François Lagunas, Alexander Rush, and Thomas Wolf. Datasets: A community library for natural language processing. In *Proceedings of the 2021 Conference on Empirical Methods in Natural Language Processing: System Demonstrations*, pages 175–184, Online and Punta Cana, Dominican Republic, November 2021. Association for Computational Linguistics. URL <https://aclanthology.org/2021.emnlp-demo.21>.
- Sylvain Gugger, Lysandre Debut, Thomas Wolf, Philipp Schmid, Zachary Mueller, Sourab Mangrulkar, Marc Sun, and Benjamin Bossan. Accelerate: Training and inference at scale made simple, efficient and adaptable. <https://github.com/huggingface/accelerate>, 2022.
- Gemma Team, Morgane Riviere, Shreya Pathak, Pier Giuseppe Sessa, Cassidy Hardin, Surya Bhupatiraju, Léonard Hussenot, Thomas Mesnard, Bobak Shahriari, Alexandre Ramé, Johan Ferret, Peter Liu, Pouya Tafti, Abe Friesen, Michelle Casbon, Sabela Ramos, Ravin Kumar, Charline Le Lan, Sammy Jerome, Anton Tsitsulin, Nino Vieillard, Piotr Stanczyk, Sertan Girgin, Nikola Momchev, Matt Hoffman, Shantanu Thakoor, Jean-Bastien Grill, Behnam Neyshabur, Olivier Bachem, Alanna Walton, Aliaksei Severyn, Alicia Parrish, Aliya Ahmad, Allen Hutchison, Alvin Abdagic, Amanda Carl, Amy Shen, Andy Brock, Andy Coenen, Anthony Laforge, Antonia Paterson, Ben Bastian, Bilal Piot, Bo Wu, Brandon Royal, Charlie Chen, Chintu Kumar, Chris

- Perry, Chris Welty, Christopher A. Choquette-Choo, Danila Sinopalnikov, David Weinberger, Dimple Vijaykumar, Dominika Rogozińska, Dustin Herbison, Elisa Bandy, Emma Wang, Eric Noland, Erica Moreira, Evan Senter, Evgenii Eltyshev, Francesco Visin, Gabriel Rasskin, Gary Wei, Glenn Cameron, Gus Martins, Hadi Hashemi, Hanna Klimczak-Plucińska, Harleen Batra, Harsh Dhand, Ivan Nardini, Jacinda Mein, Jack Zhou, James Svensson, Jeff Stanway, Jetha Chan, Jin Peng Zhou, Joana Carrasqueira, Joana Iljazi, Jocelyn Becker, Joe Fernandez, Joost van Amersfoort, Josh Gordon, Josh Lipschultz, Josh Newlan, Ju yeong Ji, Kareem Mohamed, Kartikeya Badola, Kat Black, Katie Millican, Keelin McDonell, Kelvin Nguyen, Kiranbir Sodhia, Kish Greene, Lars Lowe Sjoesund, Lauren Usui, Laurent Sifre, Lena Heuermann, Leticia Lago, Lilly McNealus, Livio Baldini Soares, Logan Kilpatrick, Lucas Dixon, Luciano Martins, Machel Reid, Manvinder Singh, Mark Iverson, Martin Görner, Mat Velloso, Mateo Wirth, Matt Davidow, Matt Miller, Matthew Rahtz, Matthew Watson, Meg Risdal, Mehran Kazemi, Michael Moynihan, Ming Zhang, Minsuk Kahng, Minwoo Park, Mofi Rahman, Mohit Khatwani, Natalie Dao, Nenshad Bardoliwalla, Nesh Devanathan, Neta Dumai, Nilay Chauhan, Oscar Wahltinez, Pankil Botarda, Parker Barnes, Paul Barham, Paul Michel, Pengchong Jin, Petko Georgiev, Phil Culliton, Pradeep Kuppala, Ramona Comanescu, Ramona Merhej, Reena Jana, Reza Ardeshir Rokni, Rishabh Agarwal, Ryan Mullins, Samaneh Saadat, Sara Mc Carthy, Sarah Cogan, Sarah Perrin, Sébastien M. R. Arnold, Sebastian Krause, Shengyang Dai, Shruti Garg, Shruti Sheth, Sue Ronstrom, Susan Chan, Timothy Jordan, Ting Yu, Tom Eccles, Tom Hennigan, Tomas Kocisky, Tulsee Doshi, Vihan Jain, Vikas Yadav, Vilobh Meshram, Vishal Dharmadhikari, Warren Barkley, Wei Wei, Wenming Ye, Woohyun Han, Woosuk Kwon, Xiang Xu, Zhe Shen, Zhitao Gong, Zichuan Wei, Victor Cotruta, Phoebe Kirk, Anand Rao, Minh Giang, Ludovic Peran, Tris Warkentin, Eli Collins, Joelle Barral, Zoubin Ghahramani, Raia Hadsell, D. Sculley, Jeanine Banks, Anca Dragan, Slav Petrov, Oriol Vinyals, Jeff Dean, Demis Hassabis, Koray Kavukcuoglu, Clement Farabet, Elena Buchatskaya, Sebastian Borgeaud, Noah Fiedel, Armand Joulin, Kathleen Kenealy, Robert Dadashi, and Alek Andreev. Gemma 2: Improving open language models at a practical size, 2024. URL <https://arxiv.org/abs/2408.00118>.
- Longhui Yu, Weisen Jiang, Han Shi, Jincheng Yu, Zhengying Liu, Yu Zhang, James T Kwok, Zhenguo Li, Adrian Weller, and Weiyang Liu. Metamath: Bootstrap your own mathematical questions for large language models. *arXiv preprint arXiv:2309.12284*, 2023.
- Karl Cobbe, Vineet Kosaraju, Mohammad Bavarian, Jacob Hilton, Reiichiro Nakano, Christopher Hesse, and John Schulman. Training verifiers to solve math word problems, 2021.
- Dan Hendrycks, Collin Burns, Saurav Kadavath, Akul Arora, Steven Basart, Eric Tang, Dawn Song, and Jacob Steinhardt. Measuring mathematical problem solving with the math dataset. *NeurIPS*, 2021a.
- Dan Hendrycks, Collin Burns, Steven Basart, Andy Zou, Mantas Mazeika, Dawn Song, and Jacob Steinhardt. Measuring massive multitask language understanding. *Proceedings of the International Conference on Learning Representations (ICLR)*, 2021b.
- Jacob Austin, Augustus Odena, Maxwell Nye, Maarten Bosma, Henryk Michalewski, David Dohan, Ellen Jiang, Carrie Cai, Michael Terry, Quoc Le, et al. Program synthesis with large language models. *arXiv preprint arXiv:2108.07732*, 2021.
- Leo Gao, Jonathan Tow, Baber Abbasi, Stella Biderman, Sid Black, Anthony DiPofi, Charles Foster, Laurence Golding, Jeffrey Hsu, Alain Le Noac’h, Haonan Li, Kyle McDonell, Niklas Muennighoff, Chris Ociepa, Jason Phang, Laria Reynolds, Hailey Schoelkopf, Aviya Skowron, Lintang Sutawika,

- Eric Tang, Anish Thite, Ben Wang, Kevin Wang, and Andy Zou. A framework for few-shot language model evaluation, 07 2024. URL <https://zenodo.org/records/12608602>.
- Jaehoon Lee, Lechao Xiao, Samuel Schoenholz, Yasaman Bahri, Roman Novak, Jascha Sohl-Dickstein, and Jeffrey Pennington. Wide neural networks of any depth evolve as linear models under gradient descent. *Advances in neural information processing systems*, 32, 2019b.
- James McClelland, Bruce McNaughton, and Randall O’Reilly. Why there are complementary learning systems in the hippocampus and neocortex: Insights from the successes and failures of connectionist models of learning and memory. *Psychological review*, 102:419–57, 08 1995. doi:10.1037/0033-295X.102.3.419.
- Lucas Caccia, Eugene Belilovsky, Massimo Caccia, and Joelle Pineau. Online learned continual compression with adaptive quantization modules. In *Proceedings of the 37th International Conference on Machine Learning, ICML’20*. JMLR.org, 2020.
- Liyuan Wang, Xingxing Zhang, Kuo Yang, Longhui Yu, Chongxuan Li, Lanqing HONG, Shifeng Zhang, Zhenguo Li, Yi Zhong, and Jun Zhu. Memory replay with data compression for continual learning. In *International Conference on Learning Representations*, 2022b. URL <https://openreview.net/forum?id=a7H70ucbWaU>.
- Geoffrey E. Hinton, Oriol Vinyals, and Jeffrey Dean. Distilling the knowledge in a neural network. *CoRR*, abs/1503.02531, 2015. URL <http://arxiv.org/abs/1503.02531>.
- Heechul Jung, Jeongwoo Ju, Minju Jung, and Junmo Kim. Less-forgetful learning for domain expansion in deep neural networks. In *AAAI Conference on Artificial Intelligence*, 2017. URL <https://api.semanticscholar.org/CorpusID:19243534>.
- Ronald Kemker and Christopher Kanan. Fearnnet: Brain-inspired model for incremental learning. In *International Conference on Learning Representations*, 2018. URL <https://openreview.net/forum?id=SJ1Xmf-Rb>.
- Yue Wu, Yinpeng Chen, Lijuan Wang, Yuancheng Ye, Zicheng Liu, Yandong Guo, Zhengyou Zhang, and Yun Raymond Fu. Incremental classifier learning with generative adversarial networks. *ArXiv*, abs/1802.00853, 2018. URL <https://api.semanticscholar.org/CorpusID:3652214>.
- Rowan Zellers, Ari Holtzman, Yonatan Bisk, Ali Farhadi, and Yejin Choi. Hellaswag: Can a machine really finish your sentence? In *Proceedings of the 57th Annual Meeting of the Association for Computational Linguistics*, 2019.
- Peter Clark, Isaac Cowhey, Oren Etzioni, Tushar Khot, Ashish Sabharwal, Carissa Schoenick, and Oyvind Tafjord. Think you have solved question answering? try arc, the ai2 reasoning challenge. *ArXiv*, abs/1803.05457, 2018.
- Keisuke Sakaguchi, Ronan Le Bras, Chandra Bhagavatula, and Yejin Choi. Winogrande: An adversarial winograd schema challenge at scale. *arXiv preprint arXiv:1907.10641*, 2019.
- Yonatan Bisk, Rowan Zellers, Ronan Le Bras, Jianfeng Gao, and Yejin Choi. Piqa: Reasoning about physical commonsense in natural language. In *Thirty-Fourth AAAI Conference on Artificial Intelligence*, 2020.

Maarten Sap, Hannah Rashkin, Derek Chen, Ronan Le Bras, and Yejin Choi. Social iqa: Commonsense reasoning about social interactions. In *Proceedings of the 2019 Conference on Empirical Methods in Natural Language Processing and the 9th International Joint Conference on Natural Language Processing (EMNLP-IJCNLP)*, pages 4463–4473, 2019.

Todor Mihaylov, Peter Clark, Tushar Khot, and Ashish Sabharwal. Can a suit of armor conduct electricity? a new dataset for open book question answering. In *EMNLP*, 2018.

Appendix

Table of Contents

- Appendix A: Extended Related Work on Data-Aware Approaches
- Appendix B: Our Algorithm in the Presence of Task-Specific Model Components
- Appendix C: Proof of Proposition 4.3
- Appendix D: Proof of Theorem 7.2
- Appendix E: Difficulty in the Analysis with a General Covariance Matrix $\tilde{\Sigma}$
- Appendix F: Lemmas Used and Their Proofs
- Appendix G: Experimental Details
 - Appendix G.1: Additional Experimental Baseline Details
 - Appendix G.2: Language Model Hyper-Parameters
 - Appendix G.3: Language Model Evaluation Details
 - Appendix G.4: Vision Implementation Details
- Appendix H: Detailed Vision Results and Ablations
- Appendix I: Additional Language Model Results and Ablations
 - Appendix I.1: Extended Commonsense Reasoning Results
 - Appendix I.2: Token-wise Sample Weighting Ablations
 - Appendix I.3: Extended Weight Averaging Results

A Extended Related Work on Data-Aware Approaches

The majority of the approaches for mitigating forgetting assume task-specific knowledge access to different extents; either (a subset of) the pre-training dataset itself or some information/statistic computed from pre-training data. Below, we describe the data-aware approaches based on how they make use of task-specific knowledge.

Regularization-based methods. This line of work aims to preserve performance on previously learned tasks by keeping the (fine-tuned) model parameters close to the pre-trained model. The key idea is to introduce task-specific regularization in the fine-tuning phase which will penalize updates along the “important” directions for the old tasks [Ahn et al., 2019]. Kirkpatrick et al. [2016] introduces the elastic weight consolidation (EWC) algorithm, which estimates the important direction per-task by calculating a diagonal approximation to the Fisher information matrix (FIM), which acts as the weight matrix for the regularization term. Several variants of EWC have been subsequently proposed [Schwarz et al., 2018, Ritter et al., 2018, Lee et al., 2020, Liu et al., 2018]. Zenke et al. [2017], Aljundi et al. [2018] adopt online strategies to infer the importance of each parameter by their variational effect on the model outputs. In a spirit similar to EWC, Lee et al. [2017] incrementally matches the posterior of the pre-trained model and the new task by assuming Gaussian posteriors.

Optimization-driven methods. Another perspective to mitigating forgetting is guiding the optimization process by constraining the algorithms directly as opposed to manipulating the loss function. The core idea is to keep track of “important directions” for the old tasks, and train on the new task “orthogonally.” This could be done by storing prior data samples or gradients in a buffer [Lopez-Paz and Ranzato, 2017, Farajtabar et al., 2020, Chaudhry et al., 2019a] or by incrementally expanding the subspace of important directions without storing task-specific information [Zeng et al., 2019, Wang et al., 2021, 2023a].

Replay-based methods. Drawing inspiration from the complementary learning systems theory [McClelland et al., 1995], a more direct approach is to introduce samples from old tasks into the training process for the new task. Samples are selected in a streaming fashion or by manually crafting a subset on demand, stored in dedicated buffers and replayed during the fine-tuning. The intuition is that the task-specific representations are refreshed periodically through historical data.

Replay-based methods consist of two fundamental components: data selection and data reiteration mechanisms. When the data is received in a streaming fashion, information has to be buffered online [Riemer et al., 2019, Chaudhry et al., 2019b, Isele and Cosgun, 2018, De Lange and Tuytelaars, 2021]. In the case when datasets are available on demand, Rebuffi et al. [2017] selects samples which are “representative” of their respective class, while others focus on inducing diversity [Aljundi et al., 2019, Bang et al., 2021] and balance [Borsos et al., 2020, Tiwari et al., 2021] across buffered data. For the scenarios in which storage is limited, Caccia et al. [2020], Wang et al. [2022b] develop compression methods for buffered data.

As a complimentary component to the data selection process, how the buffered data is replayed plays a significant role in the success of such methods. A fundamental idea, which has several interpretations across the board, is knowledge distillation [Hinton et al., 2015]. Prior work argues that augmenting fine-tuning with knowledge distillation shows great performance on the forgetting front [Lopez-Paz and Ranzato, 2017, Chaudhry et al., 2019a, Rebuffi et al., 2017, Jung et al., 2017, Triki et al., 2017, Li and Hoiem, 2016, Lee et al., 2019a, Dhar et al., 2019].

An orthogonal research direction focuses on maintaining a generative model that could reliably output pseudo-samples that are representative of the dataset of the old tasks [Kemker and Kanan, 2018, Wu et al., 2018]. Note that generative approaches are prone to scalability issues and distribution shifts.

Architecture-driven methods. Another technique to limit the interference between tasks is allocating a separate trainable set of parameters per task. This could be done by initializing a sub-networks per new task [Rusu et al., 2016, Aljundi et al., 2017, Collier et al., 2020, Rajasegaran et al., 2019, Ramesh and Chaudhari, 2021, Wang et al., 2023b, 2022a], gradually expanding the parameters of a base network [Yoon et al., 2018, Ostapenko et al., 2019, Hung et al., 2019], or segregating a fixed model into task-specific subset of parameters [Mallya et al., 2018, Kang et al., 2022, Serra et al., 2018, Wortsman et al., 2020, Mallya and Lazebnik, 2017, Mustafa B Gurbuz, 2022, Jung et al., 2020]. While some parameters are task-specific, parts of the overall model could be shared to enable knowledge transfer. The main downside is that task identity must be available during inference to (de)activate relevant sub-networks, which hinders versatility. Aljundi et al. [2017] develop dedicated strategies to overcome the need for task identification by automatizing task-specific parameter activation.

B Our Algorithm in the Presence of Task-Specific Model Components

Suppose our model is parameterized by $\theta = \mathbf{U} \cup \mathbf{V}$, where \mathbf{U} is the common/shared part of the model for all tasks (i.e., this part remains the same for all tasks), and \mathbf{V} is the task-specific part of the model. In particular, in our vision experiments, the models have task-specific prediction heads (i.e., softmax layers) and batch-norm (BN). The modified version of Algorithm 1 in the presence of task-specific components is stated in Algorithm 2. The main differences from Algorithm 1 are steps (i) and (iv) – these steps optimize the task-specific part for the new task with uniform weighting. It is worth mentioning that if our model consists of task-specific prediction heads – which is the case in our vision experiments – then steps (i) and (iv) are just vanilla linear probing with the pre-trained body and the body learned after fine-tuning, respectively.

Remark B.1. *In all our vision experiments (with task-specific parts), we set $\tau = \text{median}(f_i(\mathbf{U}_*^{(1)}, \mathbf{V}_*^{(2)}))$ (similar to Remark 4.2).*

C Proof of Proposition 4.3

Proof. We wish to minimize $g(\boldsymbol{\pi}) = \sum_{i=1}^n \pi_i f_i(\boldsymbol{\theta}^*) + \tau \sum_{i=1}^n \pi_i \log \pi_i$ subject to $\sum_{i=1}^n \pi_i = 1$ and $\pi_i \geq 0$ for all $i \in [n]$. The proof is a straightforward application of Lagrangian multipliers. It is enough to enforce $\sum_{i=1}^n \pi_i = 1$ only ($\pi_i \geq 0$ for all $i \in [n]$ will also follow). For that, the Lagrangian function is:

$$J(\boldsymbol{\pi}, \lambda) = \sum_{i=1}^n \pi_i f_i(\boldsymbol{\theta}^*) + \tau \sum_{i=1}^n \pi_i \log \pi_i + \lambda \left(\sum_{i=1}^n \pi_i - 1 \right), \quad (19)$$

where λ is the Lagrangian multiplier. Now, at the optimal point $\boldsymbol{\pi}^* = [\pi_1^*, \dots, \pi_n^*]^\top$, we must have:

$$\left. \frac{\partial J}{\partial \pi_i} \right|_{\pi_i^*} = f_i(\boldsymbol{\theta}^*) + \tau (1 + \log \pi_i^*) + \lambda = 0, \quad (20)$$

Algorithm 2 Fine-tuning with Pre-trained Loss-Oriented Weighting (**FLOW**)

Input: Pre-trained model $\boldsymbol{\theta}_*^{(1)} = \mathbf{U}_*^{(1)} \cup \mathbf{V}_*^{(1)}$, dataset $\{(\mathbf{x}_i, y_i)\}_{i=1}^n$ for the new task, and temperature parameter τ .

$f_i(\mathbf{U}, \mathbf{V}) \rightarrow i^{\text{th}}$ sample's loss at $\boldsymbol{\theta} = \mathbf{U} \cup \mathbf{V}$, with a non-negative loss function (e.g., cross-entropy loss).

Step (i) Fine-tune task-specific part for new task with vanilla unweighted loss: $\mathbf{V}_*^{(2)} := \operatorname{argmin}_{\mathbf{V}} \sum_{i=1}^n f_i(\mathbf{U}_*^{(1)}, \mathbf{V})$.

Step (ii) Compute sample weights: $w_i = \exp\left(-f_i(\mathbf{U}_*^{(1)}, \mathbf{V}_*^{(2)})/\tau\right)$.

Step (iii) Fine-tune full model **with weighted loss**: $\bar{\mathbf{U}}_*^{(2)}, \bar{\mathbf{V}}_*^{(2)} := \operatorname{argmin}_{\mathbf{U}, \mathbf{V}} \sum_{i=1}^n w_i f_i(\mathbf{U}, \mathbf{V})$.

Step (iv) Fine-tune task-specific part for new task *using the learned common part* with vanilla unweighted loss: $\hat{\mathbf{V}}_*^{(2)} := \operatorname{argmin}_{\mathbf{V}} \sum_{i=1}^n f_i(\bar{\mathbf{U}}_*^{(2)}, \mathbf{V})$.

Output: New model for

- Original/pre-training task is $\hat{\boldsymbol{\theta}}_*^{(1)} = \bar{\mathbf{U}}_*^{(2)} \cup \mathbf{V}_*^{(1)}$.
 - New/fine-tuning task is $\hat{\boldsymbol{\theta}}_*^{(2)} = \bar{\mathbf{U}}_*^{(2)} \cup \hat{\mathbf{V}}_*^{(2)}$.
-

for all $i \in [n]$. Simplifying, we get:

$$\pi_i^* = \frac{1}{Z} \exp\left(-\frac{f_i(\boldsymbol{\theta}^*)}{\tau}\right), \quad (21)$$

where $Z = \exp\left(\left(1 + \frac{\lambda}{\tau}\right)\right)$ is the normalizing constant. To have $\sum_{i=1}^n \pi_i = 1$, we get $Z = \sum_{j=1}^n \exp\left(-\frac{f_j(\mathbf{W}^*)}{\tau}\right)$. Also, note that we are good with the non-negativity constraints. \square

D Proof of Theorem 7.2

Proof. Note that:

$$\widehat{\operatorname{err}}_2(\hat{\boldsymbol{\theta}}) = (\hat{\boldsymbol{\theta}} - \tilde{\boldsymbol{\theta}}_*)^\top \mathbb{E}_{\tilde{\mathcal{D}}} \left[w(\tilde{\mathbf{x}}, \tilde{y}) \tilde{\mathbf{x}} \tilde{\mathbf{x}}^\top \right] (\hat{\boldsymbol{\theta}} - \tilde{\boldsymbol{\theta}}_*). \quad (22)$$

Also, after plugging in $\tilde{y} = \langle \tilde{\boldsymbol{\theta}}_*, \tilde{\mathbf{x}} \rangle$, we get:

$$w(\tilde{\mathbf{x}}, \tilde{y}) = \exp\left(-\frac{(\langle \boldsymbol{\theta}_* - \tilde{\boldsymbol{\theta}}_*, \tilde{\mathbf{x}} \rangle)^2}{\tau}\right).$$

Recall $\mathbf{e} := \boldsymbol{\theta}_* - \tilde{\boldsymbol{\theta}}_*$ and $\bar{\mathbf{e}} := \frac{\mathbf{e}}{\|\mathbf{e}\|_2}$. Suppose $\tau = \alpha \|\mathbf{e}\|_2^2$, for some $\alpha > 0$. Then $w(\tilde{\mathbf{x}}, \tilde{y}) = \exp\left(-\frac{(\langle \bar{\mathbf{e}}, \tilde{\mathbf{x}} \rangle)^2}{\alpha}\right)$, and we can focus on

$$\tilde{\boldsymbol{\Sigma}}' := \mathbb{E}_{\tilde{\mathbf{x}} \sim \tilde{\mathcal{P}}} \left[\exp\left(-\frac{(\langle \bar{\mathbf{e}}, \tilde{\mathbf{x}} \rangle)^2}{\alpha}\right) \tilde{\mathbf{x}} \tilde{\mathbf{x}}^\top \right]. \quad (23)$$

Let $\mu = \left(\frac{\alpha}{\alpha+2}\right)^{1/2} = \left(\frac{\tau}{\tau+2\|\mathbf{e}\|_2^2}\right)^{1/2}$. As per Lemma F.1, we have:

$$\tilde{\Sigma}' = \mu(\mathbf{I}_d - \mathbf{Q}), \quad (24)$$

where

$$\mathbf{Q} = (1 - \mu^2)\bar{\mathbf{e}}\bar{\mathbf{e}}^\top + \rho^2(1 - \mu^2)\bar{\mathbf{e}}_\perp\bar{\mathbf{e}}_\perp^\top - \rho\mu^2(\bar{\mathbf{e}}\bar{\mathbf{e}}_\perp^\top + \bar{\mathbf{e}}_\perp\bar{\mathbf{e}}^\top). \quad (25)$$

So if we minimize $\widehat{\text{err}}_2(\hat{\boldsymbol{\theta}})$ with GD starting from $\hat{\boldsymbol{\theta}}_0 = \boldsymbol{\theta}_*$ and using a constant learning rate $\hat{\eta}$, our iterate $\hat{\boldsymbol{\theta}}_K$ at the K^{th} iteration satisfies:

$$\hat{\boldsymbol{\theta}}_K - \tilde{\boldsymbol{\theta}}_* = \left(\mathbf{I}_d - 2\hat{\eta}\tilde{\Sigma}'\right)^K (\boldsymbol{\theta}_* - \tilde{\boldsymbol{\theta}}_*) = \left(\mathbf{I}_d - 2\hat{\eta}\tilde{\Sigma}'\right)^K \mathbf{e}, \quad (26)$$

where the last step follows by recalling that $\boldsymbol{\theta}_* - \tilde{\boldsymbol{\theta}}_* = \mathbf{e}$, and $\tilde{\Sigma}'$ is given by Equation (24). \square

E Difficulty in the Analysis with a General Covariance Matrix $\tilde{\Sigma}$

We will first derive the *weighted* (fine-tuning) data covariance matrix $\tilde{\Sigma}'$ in the context of Theorem 7.2 for a general (fine-tuning) data covariance matrix $\tilde{\Sigma}$. Specifically, following the proof of Theorem 7.2, we have:

$$\tilde{\Sigma}' := \mathbb{E}_{\tilde{\mathbf{x}} \sim \mathcal{N}(\vec{0}_d, \tilde{\Sigma})} \left[\exp\left(-\frac{(\langle \mathbf{e}, \tilde{\mathbf{x}} \rangle)^2}{\tau}\right) \tilde{\mathbf{x}}\tilde{\mathbf{x}}^\top \right]. \quad (27)$$

Note that $\tilde{\mathbf{x}} = \tilde{\Sigma}^{1/2}\mathbf{z}$, where $\mathbf{z} \sim \mathcal{N}(\vec{0}_d, \mathbf{I}_d)$. Using this above, we get:

$$\tilde{\Sigma}' = \tilde{\Sigma}^{1/2} \mathbb{E} \left[\exp\left(-\frac{(\langle \mathbf{e}, \tilde{\Sigma}^{1/2}\mathbf{z} \rangle)^2}{\tau}\right) \mathbf{z}\mathbf{z}^\top \right] \tilde{\Sigma}^{1/2} = \tilde{\Sigma}^{1/2} \mathbb{E} \left[\exp\left(-\frac{(\langle \tilde{\Sigma}^{1/2}\mathbf{e}, \mathbf{z} \rangle)^2}{\tau}\right) \mathbf{z}\mathbf{z}^\top \right] \tilde{\Sigma}^{1/2}, \quad (28)$$

where the last step follows by using the symmetry of $\tilde{\Sigma}$. Let $\tau = \alpha \|\tilde{\Sigma}^{1/2}\mathbf{e}\|_2^2$ for some $\alpha > 0$. Also, let $\mathbf{r} := (\tilde{\Sigma}^{1/2}\mathbf{e}) / \|\tilde{\Sigma}^{1/2}\mathbf{e}\|_2$. In that case, we have:

$$\tilde{\Sigma}' = \tilde{\Sigma}^{1/2} \mathbf{M} \tilde{\Sigma}^{1/2}, \quad \text{where } \mathbf{M} := \mathbb{E} \left[\exp\left(-\frac{(\langle \mathbf{r}, \mathbf{z} \rangle)^2}{\alpha}\right) \mathbf{z}\mathbf{z}^\top \right]. \quad (29)$$

Suppose $\{\mathbf{r}_{\perp,j}\}_{j=1}^{d-1}$ is an orthonormal basis for the subspace of \mathbb{R}^d orthogonal to \mathbf{r} ; so $\langle \mathbf{r}_{\perp,j}, \mathbf{r} \rangle = 0 \forall j \in [d-1]$ and $\langle \mathbf{r}_{\perp,j}, \mathbf{r}_{\perp,k} \rangle = \mathbf{1}(j=k) \forall j, k \in [d-1]$. Note that $\{\mathbf{r}, \mathbf{r}_{\perp,1}, \dots, \mathbf{r}_{\perp,d-1}\}$ forms an orthonormal basis for \mathbb{R}^d . Then, as per Lemma F.5, we have that \mathbf{r} is an eigenvector of \mathbf{M} with eigenvalue $\left(\frac{\alpha}{\alpha+2}\right)^{3/2}$, and each $\mathbf{r}_{\perp,j}$ is an eigenvector of \mathbf{M} with eigenvalue $\left(\frac{\alpha}{\alpha+2}\right)^{1/2}$. For brevity, let $\mu = \left(\frac{\alpha}{\alpha+2}\right)^{1/2}$. Then, we can write:

$$\mathbf{M} = \mu^3 \mathbf{r}\mathbf{r}^\top + \mu \sum_{j=1}^{d-1} \mathbf{r}_{\perp,j} \mathbf{r}_{\perp,j}^\top = \mu^3 \mathbf{r}\mathbf{r}^\top + \mu (\mathbf{I}_d - \mathbf{r}\mathbf{r}^\top), \quad (30)$$

where the last step follows because $\{\mathbf{r}, \mathbf{r}_{\perp,1}, \dots, \mathbf{r}_{\perp,d-1}\}$ forms an orthonormal basis for \mathbb{R}^d , due to which $\mathbf{r}\mathbf{r}^\top + \sum_{j=1}^{d-1} \mathbf{r}_{\perp,j} \mathbf{r}_{\perp,j}^\top = \mathbf{I}_d$. Simplifying Equation (30) a bit, we get:

$$\mathbf{M} = \mu (\mathbf{I}_d - (1 - \mu^2) \mathbf{r}\mathbf{r}^\top). \quad (31)$$

Plugging this into Equation (29) and recalling that $\mathbf{r} := (\tilde{\Sigma}^{1/2}\mathbf{e})/\|\tilde{\Sigma}^{1/2}\mathbf{e}\|_2$, we get:

$$\tilde{\Sigma}' = \mu\mathbf{B}, \text{ where } \mathbf{B} := \left(\tilde{\Sigma} - (1 - \mu^2) \frac{\tilde{\Sigma}\mathbf{e}\mathbf{e}^\top\tilde{\Sigma}}{\mathbf{e}^\top\tilde{\Sigma}\mathbf{e}} \right). \quad (32)$$

Equation (32) is the weighted covariance matrix for a general $\tilde{\Sigma}$.

Remark E.1 (Difficulty with general $\tilde{\Sigma}$). *It is hard to proceed with the analysis after this point because it is difficult to characterize the eigen-spectrum of \mathbf{B} in general, without assuming any relation between $\tilde{\Sigma}$ and \mathbf{e} . This is what we meant in Remark 7.1.*

F Lemmas Used and their Proofs

Lemma F.1. *In the proof of Theorem 7.2, recall that $\tau = \alpha\|\mathbf{e}\|_2^2$. Then, we have:*

$$\tilde{\Sigma}' := \mathbb{E}_{\tilde{\mathbf{x}} \sim \tilde{\rho}} \left[\exp \left(- \frac{(\langle \bar{\mathbf{e}}, \tilde{\mathbf{x}} \rangle)^2}{\alpha} \right) \tilde{\mathbf{x}}\tilde{\mathbf{x}}^\top \right] = \mu \left(\mathbf{I}_d - (1 - \mu^2)\bar{\mathbf{e}}\bar{\mathbf{e}}^\top - \rho^2(1 - \mu^2)\bar{\mathbf{e}}_\perp\bar{\mathbf{e}}_\perp^\top + \rho\mu^2(\bar{\mathbf{e}}\bar{\mathbf{e}}_\perp^\top + \bar{\mathbf{e}}_\perp\bar{\mathbf{e}}^\top) \right),$$

$$\text{where } \mu = \left(\frac{\alpha}{\alpha+2} \right)^{1/2} = \left(\frac{\tau}{\tau+2\|\mathbf{e}\|_2^2} \right)^{1/2}.$$

Proof. Recall that $\bar{\mathbf{e}}$ and $\bar{\mathbf{e}}_\perp$ are orthogonal to each other and both are unit-norm. Suppose $\{\bar{\mathbf{e}}_{\perp,3}, \bar{\mathbf{e}}_{\perp,4}, \dots, \bar{\mathbf{e}}_{\perp,d}\}$ is an orthonormal basis for the $(d-2)$ -dimensional subspace of \mathbb{R}^d orthogonal to $\bar{\mathbf{e}}$ and $\bar{\mathbf{e}}_\perp$. Thus, $\{\bar{\mathbf{e}}, \bar{\mathbf{e}}_\perp, \bar{\mathbf{e}}_{\perp,3}, \bar{\mathbf{e}}_{\perp,4}, \dots, \bar{\mathbf{e}}_{\perp,d}\}$ is an orthonormal basis for \mathbb{R}^d . Then using Lemma F.2, we can write:

$$\tilde{\mathbf{x}} = z_1\bar{\mathbf{e}} + \left(\rho z_1 + \sqrt{1 - \rho^2}z_2 \right) \bar{\mathbf{e}}_\perp + \sum_{j=3}^d z_j \bar{\mathbf{e}}_{\perp,j}, \quad (33)$$

where $\{z_j\}_{j=1}^d \stackrel{\text{iid}}{\sim} \mathcal{N}(0, 1)$.

Using independence and zero-mean nature of $\{z_j\}_{j=1}^d$, we get:

$$\begin{aligned} \tilde{\Sigma}' &= \underbrace{\mathbb{E} \left[\exp \left(- \frac{z_1^2}{\alpha} \right) z_1^2 \right]}_{:=T_1} \bar{\mathbf{e}}\bar{\mathbf{e}}^\top + \underbrace{\mathbb{E} \left[\exp \left(- \frac{z_1^2}{\alpha} \right) z_1 \left(\rho z_1 + \sqrt{1 - \rho^2}z_2 \right) \right]}_{:=T_2} (\bar{\mathbf{e}}\bar{\mathbf{e}}_\perp^\top + \bar{\mathbf{e}}_\perp\bar{\mathbf{e}}^\top) \\ &\quad + \underbrace{\mathbb{E} \left[\exp \left(- \frac{z_1^2}{\alpha} \right) \left(\rho z_1 + \sqrt{1 - \rho^2}z_2 \right)^2 \right]}_{:=T_3} \bar{\mathbf{e}}_\perp\bar{\mathbf{e}}_\perp^\top + \sum_{j=3}^d \underbrace{\mathbb{E} \left[\exp \left(- \frac{z_1^2}{\alpha} \right) \right]}_{:=T_4} \underbrace{\mathbb{E} [z_j^2]}_{=1} \bar{\mathbf{e}}_{\perp,j}\bar{\mathbf{e}}_{\perp,j}^\top. \end{aligned} \quad (34)$$

Note that (we use the independence of z_1 and z_2):

$$T_2 = \rho T_1 + \sqrt{1 - \rho^2} \mathbb{E} \left[\exp \left(- \frac{z_1^2}{\alpha} \right) z_1 \right] \underbrace{\mathbb{E} [z_2]}_{=0} = \rho T_1, \quad (35)$$

and

$$T_3 = \rho^2 T_1 + 2\rho\sqrt{1 - \rho^2} \left[\exp \left(- \frac{z_1^2}{\alpha} \right) z_1 \right] \underbrace{\mathbb{E} [z_2]}_{=0} + (1 - \rho^2) T_4 \underbrace{\mathbb{E} [z_2^2]}_{=1} = \rho^2 T_1 + (1 - \rho^2) T_4. \quad (36)$$

In the above two equations, we have again used the independence of z_1 and z_2 . Now we will compute T_1 and T_4 . We have:

$$T_1 = \left(\frac{1}{\sqrt{2\pi}} \int_{-\infty}^{\infty} z_1^2 \exp\left(-z_1^2 \left(\frac{1}{\alpha} + \frac{1}{2}\right)\right) dz_1 \right) = \left(\frac{\alpha}{\alpha+2}\right)^{3/2}, \quad (37)$$

and

$$T_4 = \left(\frac{1}{\sqrt{2\pi}} \int_{-\infty}^{\infty} \exp\left(-z_1^2 \left(\frac{1}{\alpha} + \frac{1}{2}\right)\right) dz_1 \right) = \left(\frac{\alpha}{\alpha+2}\right)^{1/2}. \quad (38)$$

Recall that $\mu = \left(\frac{\alpha}{\alpha+2}\right)^{1/2}$. Plugging this into Equations (35) to (38) gives us:

$$T_1 = \mu^3, T_2 = \rho\mu^3, T_3 = \rho^2\mu^3 + (1 - \rho^2)\mu, \text{ and } T_4 = \mu. \quad (39)$$

Plugging this into Equation (34) gives us:

$$\tilde{\Sigma}' = \mu^3 \bar{\mathbf{e}}\bar{\mathbf{e}}^\top + \rho\mu^3(\bar{\mathbf{e}}\bar{\mathbf{e}}_\perp^\top + \bar{\mathbf{e}}_\perp\bar{\mathbf{e}}^\top) + \left(\rho^2\mu^3 + (1 - \rho^2)\mu\right)\bar{\mathbf{e}}_\perp\bar{\mathbf{e}}_\perp^\top + \mu \sum_{j=3}^d \bar{\mathbf{e}}_{\perp,j}\bar{\mathbf{e}}_{\perp,j}^\top. \quad (40)$$

Recall that $\{\bar{\mathbf{e}}, \bar{\mathbf{e}}_\perp, \bar{\mathbf{e}}_{\perp,3}, \bar{\mathbf{e}}_{\perp,4}, \dots, \bar{\mathbf{e}}_{\perp,d}\}$ is an orthonormal basis for \mathbb{R}^d . Thus, $\sum_{j=3}^d \bar{\mathbf{e}}_{\perp,j}\bar{\mathbf{e}}_{\perp,j}^\top = \mathbf{I}_d - \bar{\mathbf{e}}\bar{\mathbf{e}}^\top - \bar{\mathbf{e}}_\perp\bar{\mathbf{e}}_\perp^\top$. Using this above, we get:

$$\tilde{\Sigma}' = \mu \left(\mathbf{I}_d - (1 - \mu^2)\bar{\mathbf{e}}\bar{\mathbf{e}}^\top - \rho^2(1 - \mu^2)\bar{\mathbf{e}}_\perp\bar{\mathbf{e}}_\perp^\top + \rho\mu^2(\bar{\mathbf{e}}\bar{\mathbf{e}}_\perp^\top + \bar{\mathbf{e}}_\perp\bar{\mathbf{e}}^\top) \right). \quad (41)$$

This finishes the proof. \square

Lemma F.2. *Suppose $\{\bar{\mathbf{e}}, \bar{\mathbf{e}}_\perp, \bar{\mathbf{e}}_{\perp,3}, \bar{\mathbf{e}}_{\perp,4}, \dots, \bar{\mathbf{e}}_{\perp,d}\}$ is an orthonormal basis for \mathbb{R}^d . If $\tilde{\mathbf{x}} \sim \mathcal{N}(\tilde{\mathbf{0}}_d, \tilde{\Sigma})$, then we can write:*

$$\tilde{\mathbf{x}} = z_1\bar{\mathbf{e}} + \left(\rho z_1 + \sqrt{1 - \rho^2}z_2\right)\bar{\mathbf{e}}_\perp + \sum_{j=3}^d z_j\bar{\mathbf{e}}_{\perp,j}, \quad (42)$$

where $\{z_j\}_{j=1}^d \stackrel{\text{iid}}{\sim} \mathcal{N}(0, 1)$.

Proof. If $\tilde{\mathbf{x}}$ is as per Equation (42), then clearly $\tilde{\mathbf{x}}$ is a zero-mean Gaussian. All that remains to show is that

$$\mathbb{E}[\tilde{\mathbf{x}}\tilde{\mathbf{x}}^\top] = \tilde{\Sigma} = \mathbf{I}_d + \rho(\bar{\mathbf{e}}\bar{\mathbf{e}}_\perp^\top + \bar{\mathbf{e}}_\perp\bar{\mathbf{e}}^\top).$$

Using independence and zero-mean nature of $\{z_j\}_{j=1}^d$, we get:

$$\begin{aligned} \mathbb{E}[\tilde{\mathbf{x}}\tilde{\mathbf{x}}^\top] &= \underbrace{\mathbb{E}[z_1^2]}_{=1} \bar{\mathbf{e}}\bar{\mathbf{e}}^\top + \underbrace{\mathbb{E}\left[z_1\left(\rho z_1 + \sqrt{1 - \rho^2}z_2\right)\right]}_{:=\text{(A)}} (\bar{\mathbf{e}}\bar{\mathbf{e}}_\perp^\top + \bar{\mathbf{e}}_\perp\bar{\mathbf{e}}^\top) + \underbrace{\mathbb{E}\left[\left(\rho z_1 + \sqrt{1 - \rho^2}z_2\right)^2\right]}_{:=\text{(B)}} \bar{\mathbf{e}}_\perp\bar{\mathbf{e}}_\perp^\top \\ &\quad + \sum_{j=3}^d \underbrace{\mathbb{E}[z_j^2]}_{=1} \bar{\mathbf{e}}_{\perp,j}\bar{\mathbf{e}}_{\perp,j}^\top. \end{aligned} \quad (43)$$

Note that (we use the independence of z_1 and z_2):

$$\text{(A)} = \rho \underbrace{\mathbb{E}[z_1^2]}_{=1} + \sqrt{1 - \rho^2} \underbrace{\mathbb{E}[z_1]}_{=0} \underbrace{\mathbb{E}[z_2]}_{=0} = \rho, \quad (44)$$

and

$$(B) = \underbrace{\rho^2 \mathbb{E}[z_1^2]}_{=1} + 2\rho\sqrt{1-\rho^2} \underbrace{\mathbb{E}[z_1]}_{=0} \underbrace{\mathbb{E}[z_2]}_{=0} + (1-\rho^2) \underbrace{\mathbb{E}[z_2^2]}_{=1} = 1. \quad (45)$$

Plugging this into Equation (43), we get:

$$\mathbb{E}[\tilde{\mathbf{x}}\tilde{\mathbf{x}}^\top] = \bar{\mathbf{e}}\bar{\mathbf{e}}^\top + \rho(\bar{\mathbf{e}}\bar{\mathbf{e}}_\perp^\top + \bar{\mathbf{e}}_\perp\bar{\mathbf{e}}^\top) + \bar{\mathbf{e}}_\perp\bar{\mathbf{e}}_\perp^\top + \sum_{j=3}^d \bar{\mathbf{e}}_{\perp,j}\bar{\mathbf{e}}_{\perp,j}^\top. \quad (46)$$

Recall that $\{\bar{\mathbf{e}}, \bar{\mathbf{e}}_\perp, \bar{\mathbf{e}}_{\perp,3}, \bar{\mathbf{e}}_{\perp,4}, \dots, \bar{\mathbf{e}}_{\perp,d}\}$ is an orthonormal basis for \mathbb{R}^d . Thus, $\sum_{j=3}^d \bar{\mathbf{e}}_{\perp,j}\bar{\mathbf{e}}_{\perp,j}^\top = \mathbf{I}_d - \bar{\mathbf{e}}\bar{\mathbf{e}}^\top - \bar{\mathbf{e}}_\perp\bar{\mathbf{e}}_\perp^\top$. Using this above, we get:

$$\mathbb{E}[\tilde{\mathbf{x}}\tilde{\mathbf{x}}^\top] = \mathbf{I}_d + \rho(\bar{\mathbf{e}}\bar{\mathbf{e}}_\perp^\top + \bar{\mathbf{e}}_\perp\bar{\mathbf{e}}^\top) = \tilde{\Sigma}. \quad (47)$$

This finishes the proof. \square

Lemma F.3. *Recall that*

$$\mathbf{Q} = (1-\mu^2)\bar{\mathbf{e}}\bar{\mathbf{e}}^\top + \rho^2(1-\mu^2)\bar{\mathbf{e}}_\perp\bar{\mathbf{e}}_\perp^\top - \rho\mu^2(\bar{\mathbf{e}}\bar{\mathbf{e}}_\perp^\top + \bar{\mathbf{e}}_\perp\bar{\mathbf{e}}^\top).$$

Let

$$\mu = \sqrt{\frac{\beta(1-\rho^2)}{(1+\beta)(1-\beta\rho^2)}}$$

for some $\beta \in (0, 1]$. In that case, the eigenvalues of \mathbf{Q} are:

$$\hat{\lambda}_1 = \frac{1+\beta\rho^2}{1+\beta} \text{ and } \hat{\lambda}_2 = \rho^2 \left(\frac{1-\beta}{1-\beta\rho^2} \right),$$

and the corresponding eigenvectors are:

$$\hat{\mathbf{v}}_1 = \frac{1}{\sqrt{1+\beta^2\rho^2}}\bar{\mathbf{e}} - \frac{\beta\rho}{\sqrt{1+\beta^2\rho^2}}\bar{\mathbf{e}}_\perp \text{ and } \hat{\mathbf{v}}_2 = -\frac{\beta\rho}{\sqrt{1+\beta^2\rho^2}}\bar{\mathbf{e}} - \frac{1}{\sqrt{1+\beta^2\rho^2}}\bar{\mathbf{e}}_\perp.$$

Proof. \mathbf{Q} is a rank-2 matrix and its two eigenvectors will be in the span of $\bar{\mathbf{e}}$ and $\bar{\mathbf{e}}_\perp$. In particular, an eigenvector of \mathbf{Q} is of the form $[\bar{\mathbf{e}}, \bar{\mathbf{e}}_\perp]\mathbf{b}$, where $\mathbf{b} \in \mathbb{R}^{2 \times 1}$ is an eigenvector of the 2×2 matrix:

$$\mathbf{A} := \begin{bmatrix} (1-\mu^2) & -\rho\mu^2 \\ -\rho\mu^2 & \rho^2(1-\mu^2) \end{bmatrix}. \quad (48)$$

Also, the corresponding eigenvalues of \mathbf{Q} are the corresponding eigenvalues of \mathbf{A} . It can be verified that the eigenvalues of \mathbf{A} are:

$$\hat{\lambda}_1 = \frac{(1+\rho^2)(1-\mu^2)}{2} + \sqrt{\frac{(1-\rho^2)^2(1-\mu^2)^2}{4} + \rho^2\mu^4}. \quad (49)$$

and

$$\hat{\lambda}_2 = \frac{(1+\rho^2)(1-\mu^2)}{2} - \sqrt{\frac{(1-\rho^2)^2(1-\mu^2)^2}{4} + \rho^2\mu^4}. \quad (50)$$

The corresponding eigenvectors of \mathbf{A} are:

$$\widehat{\mathbf{b}}_1 = \frac{1}{\sqrt{b_{1,1}^2 + b_{1,2}^2}} \begin{bmatrix} b_{1,1} \\ b_{1,2} \end{bmatrix} \quad (51)$$

where $b_{1,1} = \frac{(1-\rho^2)(1-\mu^2)}{2} + \sqrt{\frac{(1-\rho^2)^2(1-\mu^2)^2}{4} + \rho^2\mu^4}$ and $b_{1,2} = -\rho\mu^2$, and

$$\widehat{\mathbf{b}}_2 = \frac{1}{\sqrt{b_{2,1}^2 + b_{2,2}^2}} \begin{bmatrix} b_{2,1} \\ b_{2,2} \end{bmatrix}, \quad (52)$$

where $b_{2,1} = \frac{(1-\rho^2)(1-\mu^2)}{2} - \sqrt{\frac{(1-\rho^2)^2(1-\mu^2)^2}{4} + \rho^2\mu^4}$ and $b_{2,2} = -\rho\mu^2$. Thus, the eigenvalues of \mathbf{Q} are $\widehat{\lambda}_1$ and $\widehat{\lambda}_2$; the corresponding eigenvectors are $\widehat{\mathbf{v}}_1 = [\bar{\mathbf{e}}, \bar{\mathbf{e}}_\perp] \widehat{\mathbf{b}}_1$ and $\widehat{\mathbf{v}}_2 = [\bar{\mathbf{e}}, \bar{\mathbf{e}}_\perp] \widehat{\mathbf{b}}_2$. Note that:

$$\frac{(1-\rho^2)(1-\mu^2)}{2} \leq \sqrt{\frac{(1-\rho^2)^2(1-\mu^2)^2}{4} + \rho^2\mu^4} \leq \frac{(1-\rho^2)(1-\mu^2)}{2} + \rho\mu^2.$$

Let us set $\sqrt{\frac{(1-\rho^2)^2(1-\mu^2)^2}{4} + \rho^2\mu^4} = \frac{(1-\rho^2)(1-\mu^2)}{2} + \beta\rho^2\mu^2$, for some $\beta \in (0, 1]$. That gives us:

$$\mu = \sqrt{\frac{\beta(1-\rho^2)}{(1+\beta)(1-\beta\rho^2)}}. \quad (53)$$

In that case, we have:

$$\widehat{\lambda}_1 = \frac{1+\beta\rho^2}{1+\beta} \text{ and } \widehat{\lambda}_2 = \rho^2 \left(\frac{1-\beta}{1-\beta\rho^2} \right). \quad (54)$$

Also,

$$b_{1,1} = \frac{1-\rho^2}{(1+\beta)(1-\beta\rho^2)}, b_{1,2} = b_{2,2} = -\frac{\beta\rho(1-\rho^2)}{(1+\beta)(1-\beta\rho^2)}, \text{ and } b_{2,1} = -\frac{\beta^2\rho^2(1-\rho^2)}{(1+\beta)(1-\beta\rho^2)}. \quad (55)$$

Therefore,

$$\widehat{\mathbf{b}}_1 = \frac{1}{\sqrt{1+\beta^2\rho^2}} \begin{bmatrix} 1 \\ -\beta\rho \end{bmatrix} \text{ and } \widehat{\mathbf{b}}_2 = \frac{1}{\sqrt{1+\beta^2\rho^2}} \begin{bmatrix} -\beta\rho \\ -1 \end{bmatrix}. \quad (56)$$

Recall that the eigenvalues of \mathbf{Q} are $\widehat{\lambda}_1$ and $\widehat{\lambda}_2$, and the corresponding eigenvectors are

$$\widehat{\mathbf{v}}_1 = [\bar{\mathbf{e}}, \bar{\mathbf{e}}_\perp] \widehat{\mathbf{b}}_1 = \frac{1}{\sqrt{1+\beta^2\rho^2}} \bar{\mathbf{e}} - \frac{\beta\rho}{\sqrt{1+\beta^2\rho^2}} \bar{\mathbf{e}}_\perp \text{ and } \widehat{\mathbf{v}}_2 = [\bar{\mathbf{e}}, \bar{\mathbf{e}}_\perp] \widehat{\mathbf{b}}_2 = -\frac{\beta\rho}{\sqrt{1+\beta^2\rho^2}} \bar{\mathbf{e}} - \frac{1}{\sqrt{1+\beta^2\rho^2}} \bar{\mathbf{e}}_\perp.$$

Finally, recall that $\mu = \sqrt{\frac{\beta(1-\rho^2)}{(1+\beta)(1-\beta\rho^2)}}$. \square

Lemma F.4. Recall that the averaged model with parameter ω as defined in Equation (16) was

$$\boldsymbol{\theta}_{\text{avg}}(\omega) = \omega\boldsymbol{\theta}_* + (1-\omega)\widetilde{\boldsymbol{\theta}}_* = \widetilde{\boldsymbol{\theta}}_* + \omega\mathbf{e}.$$

We have:

$$\min_{\omega \in [0,1]} \text{err}_{\text{tot}}(\boldsymbol{\theta}_{\text{avg}}(\omega)) = \left(\frac{\bar{\mathbf{e}}^\top \boldsymbol{\Sigma} \bar{\mathbf{e}}}{\bar{\mathbf{e}}^\top \boldsymbol{\Sigma} \bar{\mathbf{e}} + 1} \right) \|\mathbf{e}\|_2^2, \quad (57)$$

where recall that $\boldsymbol{\Sigma}$ is the covariance matrix of the pre-training data.

Proof. We have:

$$\begin{aligned} \text{err}_{\text{tot}}(\boldsymbol{\theta}_{\text{avg}}(\omega)) &= \text{err}_1(\boldsymbol{\theta}_{\text{avg}}(\omega)) + \text{err}_2(\boldsymbol{\theta}_{\text{avg}}(\omega)) \\ &= (\boldsymbol{\theta}_{\text{avg}}(\omega) - \boldsymbol{\theta}_*)^\top \boldsymbol{\Sigma} (\boldsymbol{\theta}_{\text{avg}}(\omega) - \boldsymbol{\theta}_*) + (\boldsymbol{\theta}_{\text{avg}}(\omega) - \tilde{\boldsymbol{\theta}}_*)^\top \tilde{\boldsymbol{\Sigma}} (\boldsymbol{\theta}_{\text{avg}}(\omega) - \tilde{\boldsymbol{\theta}}_*). \end{aligned} \quad (58)$$

Plugging in the value of $\boldsymbol{\theta}_{\text{avg}}(\omega)$ and using the value of $\tilde{\boldsymbol{\Sigma}}$ from Equation (3), we get:

$$\text{err}_{\text{tot}}(\boldsymbol{\theta}_{\text{avg}}(\omega)) = (1 - \omega)^2 \mathbf{e}^\top \boldsymbol{\Sigma} \mathbf{e} + \omega^2 \|\mathbf{e}\|_2^2. \quad (59)$$

It can be verified (with elementary calculus) that the optimal value of ω that minimizes the RHS in Equation (59) is $\omega^* = \frac{\mathbf{e}^\top \boldsymbol{\Sigma} \mathbf{e}}{\mathbf{e}^\top \boldsymbol{\Sigma} \mathbf{e} + \|\mathbf{e}\|_2^2}$. Plugging this into Equation (59) and simplifying a bit yields the desired result. \square

Lemma F.5. *Suppose $\alpha > 0$ and $\mathbf{r} \in \mathbb{R}^d$ is a unit-norm vector, i.e., $\|\mathbf{r}\|_2 = 1$. Let*

$$\mathbf{M} := \mathbb{E} \left[\exp \left(- \frac{(\langle \mathbf{r}, \mathbf{z} \rangle)^2}{\alpha} \right) \mathbf{z} \mathbf{z}^\top \right],$$

where $\mathbf{z} \sim \mathcal{N}(\vec{0}_d, \mathbf{I}_d)$. \mathbf{r} is an eigenvector of \mathbf{M} with eigenvalue $(\frac{\alpha}{\alpha+2})^{3/2}$. Further, the eigenvectors of \mathbf{M} in the subspace of \mathbb{R}^d orthogonal to \mathbf{r} all have eigenvalues $(\frac{\alpha}{\alpha+2})^{1/2}$.

Proof. We have:

$$\mathbb{E}[\mathbf{M}\mathbf{r}] = \mathbb{E} \left[\exp \left(- \frac{(\langle \mathbf{r}, \mathbf{z} \rangle)^2}{\alpha} \right) \langle \mathbf{r}, \mathbf{z} \rangle \mathbf{z} \right]. \quad (60)$$

Suppose $\{\mathbf{r}_{\perp,j}\}_{j=1}^{d-1}$ is an orthonormal basis for the subspace orthogonal to \mathbf{r} ; so $\langle \mathbf{r}_{\perp,j}, \mathbf{r} \rangle = 0 \forall j \in [d-1]$ and $\langle \mathbf{r}_{\perp,j}, \mathbf{r}_{\perp,k} \rangle = \mathbf{1}(j=k) \forall j, k \in [d-1]$. Then, note that:

$$\mathbf{z} = \langle \mathbf{r}, \mathbf{z} \rangle \mathbf{r} + \sum_{j=1}^{d-1} \langle \mathbf{r}_{\perp,j}, \mathbf{z} \rangle \mathbf{r}_{\perp,j}. \quad (61)$$

Since $\mathbf{z} \sim \mathcal{N}(\vec{0}_d, \mathbf{I}_d)$, $\langle \mathbf{r}, \mathbf{z} \rangle$ and $\{\langle \mathbf{r}_{\perp,j}, \mathbf{z} \rangle\}_{j=1}^{d-1}$ are i.i.d. $\mathcal{N}(0, 1)$. Using all of this in Equation (60), we get:

$$\mathbb{E}[\mathbf{M}\mathbf{r}] = \mathbb{E} \left[\exp \left(- \frac{(\langle \mathbf{r}, \mathbf{z} \rangle)^2}{\alpha} \right) (\langle \mathbf{r}, \mathbf{z} \rangle)^2 \right] \mathbf{r} + \underbrace{\sum_{j=1}^{d-1} \mathbb{E} \left[\exp \left(- \frac{(\langle \mathbf{r}, \mathbf{z} \rangle)^2}{\alpha} \right) \langle \mathbf{r}, \mathbf{z} \rangle \langle \mathbf{r}_{\perp,j}, \mathbf{z} \rangle \right]}_{=0 \text{ } (\langle \mathbf{r}, \mathbf{z} \rangle \text{ and } \langle \mathbf{r}_{\perp,j}, \mathbf{z} \rangle \text{ are independent})} \mathbf{r}_{\perp,j} \quad (62)$$

$$= \mathbb{E}_{Z \sim \mathcal{N}(0,1)} \left[\exp \left(- \frac{Z^2}{\alpha} \right) Z^2 \right] \mathbf{r} \quad (\text{because } \langle \mathbf{r}, \mathbf{z} \rangle \sim \mathcal{N}(0, 1)) \quad (63)$$

$$= \left(\frac{1}{\sqrt{2\pi}} \int_{-\infty}^{\infty} z^2 \exp \left(- z^2 \left(\frac{1}{\alpha} + \frac{1}{2} \right) \right) dz \right) \mathbf{r} \quad (64)$$

$$= \left(\frac{\alpha}{\alpha + 2} \right)^{3/2} \mathbf{r}. \quad (65)$$

So \mathbf{r} is an eigenvector of \mathbf{M} with eigenvalue $(\frac{\alpha}{\alpha+2})^{3/2}$.

Next, note that:

$$\begin{aligned} \mathbb{E}[\mathbf{M}\mathbf{r}_{\perp,1}] &= \underbrace{\mathbb{E}\left[\exp\left(-\frac{(\langle\mathbf{r},\mathbf{z}\rangle)^2}{\alpha}\right)\langle\mathbf{r}_{\perp,1},\mathbf{z}\rangle\langle\mathbf{r},\mathbf{z}\rangle\right]}_{=0}\mathbf{r} + \mathbb{E}\left[\exp\left(-\frac{(\langle\mathbf{r},\mathbf{z}\rangle)^2}{\alpha}\right)(\langle\mathbf{r}_{\perp,1},\mathbf{z}\rangle)^2\right]\mathbf{r}_{\perp,1} \\ &\quad + \underbrace{\sum_{j=2}^{d-1}\mathbb{E}\left[\exp\left(-\frac{(\langle\mathbf{r},\mathbf{z}\rangle)^2}{\alpha}\right)\langle\mathbf{r}_{\perp,1},\mathbf{z}\rangle\langle\mathbf{r}_{\perp,j},\mathbf{z}\rangle\right]}_{=0}\mathbf{r}_{\perp,j}. \end{aligned} \quad (66)$$

In the above equation, the first and last terms are 0 because $\langle\mathbf{r},\mathbf{z}\rangle$ and $\{\langle\mathbf{r}_{\perp,j},\mathbf{z}\rangle\}_{j=1}^{d-1}$ are i.i.d. $\mathcal{N}(0,1)$; using this fact again, we get:

$$\mathbb{E}[\mathbf{M}\mathbf{r}_{\perp,1}] = \mathbb{E}_{Z\sim\mathcal{N}(0,1)}\left[\exp\left(-\frac{Z^2}{\alpha}\right)\right]\underbrace{\mathbb{E}_{\bar{Z}\sim\mathcal{N}(0,1)}[\bar{Z}^2]}_{=1}\mathbf{r}_{\perp,1} \quad (67)$$

$$= \left(\frac{1}{\sqrt{2\pi}}\int_{-\infty}^{\infty}\exp\left(-z^2\left(\frac{1}{\alpha}+\frac{1}{2}\right)\right)dz\right)\mathbf{r}_{\perp,1} \quad (68)$$

$$= \left(\frac{\alpha}{\alpha+2}\right)^{1/2}\mathbf{r}_{\perp,1}. \quad (69)$$

Similarly, we can show that for $j = \{2, \dots, d-1\}$, we have:

$$\mathbb{E}[\mathbf{M}\mathbf{r}_{\perp,j}] = \left(\frac{\alpha}{\alpha+2}\right)^{1/2}\mathbf{r}_{\perp,j}. \quad (70)$$

So for all $j \in [d-1]$, $\mathbf{r}_{\perp,j}$ is an eigenvector of \mathbf{M} with eigenvalue $(\frac{\alpha}{\alpha+2})^{1/2}$. Thus, the eigenvectors of \mathbf{M} in the subspace orthogonal to \mathbf{r} all have eigenvalues $(\frac{\alpha}{\alpha+2})^{1/2}$. \square

G Experimental Details

In this section, we further discuss the experimental setup of FLOW’s usage in both language and vision settings, specifically covering the following:

- Appendix G.1: Baseline implementation details for both language and vision experiments
- Appendix G.2: Fine-tuning specifications for language models (baselines versus FLOW)
- Appendix G.3: Evaluation metrics breakdown for language tasks
- Appendix G.4: Training parameters for vision models (baselines versus FLOW)

G.1 Additional Experimental Baseline Details

In this section, we further discuss the baselines mentioned in Section 5.

Linear probing: In our vision experiments, we define linear probing as freezing the body of the pre-trained model, initializing a new (task-specific) head and batch normalization layers, and training only the new head and batch normalization layers.

ℓ_2 regularization: Based on Kirkpatrick et al. [2016], we perform ℓ_2 regularization as a baseline in the data-oblivious setting. Specifically, the ℓ_2 -regularized loss is:

$$\mathcal{L}(\boldsymbol{\theta}) = \sum_{i=1}^n f_i(\boldsymbol{\theta}) + \lambda \|\boldsymbol{\theta} - \boldsymbol{\theta}^*\|_2^2 \tag{71}$$

where f_i is the i^{th} sample’s loss, $\boldsymbol{\theta}^*$ is the pre-trained model, and λ is the regularization parameter. Intuitively, as λ increases, our model stays closer to the pre-trained model, mitigating forgetting at the expense of target domain performance.

LoRA [Hu et al., 2022]: Recently, Biderman et al. [2024] showed that fine-tuning language models with LoRA [Hu et al., 2022] effectively mitigates forgetting. Following a similar setup as us, Biderman et al. [2024] fine-tuned language models on MetaMathQA [Yu et al., 2023] and then evaluated the fine-tuned model on several general capability tasks, viz., HellaSwag [Zellers et al., 2019], ARC-c [Clark et al., 2018], and WinoGrande [Sakaguchi et al., 2019], and one target domain task, viz., GSM8K [Cobbe et al., 2021]. Further details about experimental hyper-parameters can be found in Appendix G.2.

WiSE-FT [Wortsman et al., 2021]: We also consider model averaging as a baseline, specifically focusing on WiSE-FT [Wortsman et al., 2021]. WiSE-FT is simply the convex combination of the model parameters shared between the two tasks, while the task-specific parts are not averaged. Specifically, we perform model averaging between the pre-trained model and the fine-tuned model. The convex combination parameter α of WiSE-FT is set to 0.5 in our experiments, as we cannot optimize α in the data-oblivious setting.

G.2 Language Model Hyper-Parameters

For both Gemma 2 2B [Team et al., 2024] and Llama 3.2 3B [Grattafiori et al., 2024], we run hyper-parameter sweeps on learning rates for each baseline. For standard fine-tuning, ℓ_2 regularization, and FLOW, we do a learning rate sweep in [1e-4, 2e-5, 1e-5, 5e-6], and for LoRA ($r = 64$) we do a sweep in [2e-4, 2e-1], following the learning rates used in Biderman et al. [2024]. We then select the learning rate that results in the best GSM8K [Cobbe et al., 2021] accuracy, oblivious to general capability metrics. We report the hyper-parameters used for our Gemma 2 2B experiments in Table 5 and for Llama 3.2 3B in Table 6.

Table 5: The hyper-parameters used to train Gemma 2 2B in our experiments. Note that the learning rate selected is based on the best results on GSM8K after fine-tuning the method on MetaMathQA.

Hyper-parameter	Standard Fine-tuning	LoRA ($r = 64$)	ℓ_2 -Reg.	FLOW (Ours)
Learning Rate	1e-5	2e-4	5e-6	5e-6
Learning Rate Scheduler		Cosine		
Batch Size		128		
Optimizer		AdamW		
Weight Decay		0.00		
Warmup Ratio		0.03		
Epochs		2		
Max Sequence Length		1024		
Seed		42		

Table 6: The hyper-parameters used to train Llama 3.2 3B in our experiments. Note that the learning rate selected is based on the best results on GSM8K after fine-tuning the method on MetaMathQA.

Hyper-parameter	Standard Fine-tuning	LoRA ($r = 64$)	ℓ_2 -Reg.	FLOW (Ours)
Learning Rate	2e-5	2e-4	1e-5	1e-5
Learning Rate Scheduler		Cosine		
Batch Size		128		
Optimizer		AdamW		
Weight Decay		0.00		
Warmup Ratio		0.03		
Epochs		2		
Max Sequence Length		1024		
Seed		42		

For our WiSE-FT model averaging experiments, we use $\alpha = 0.5$. For our LoRA experiments, we use $\alpha = r = 64$. For ℓ_2 regularization we use $\lambda = 1e - 3$ which is taken from Chen et al. [2024a]. Most training hyper-parameters for our language experiments are taken from Chen et al. [2024a], with the introduction of learning rate sweeps.

G.3 Language Model Evaluation Details

As described in Section 5.2, we create a commonsense reasoning metric composed of the following six metrics: ARC-e [Clark et al., 2018], ARC-c [Clark et al., 2018], HellaSwag [Zellers et al., 2019],

PIQA [Bisk et al., 2020], SIQA [Sap et al., 2019], and OBQA [Mihaylov et al., 2018]. On top of the commonsense metric, we evaluate MMLU [Hendrycks et al., 2021b] and MBPP [Austin et al., 2021] to estimate the general capabilities of a language model and to measure the effects of catastrophic forgetting when fine-tuning a model on MetaMathQA [Yu et al., 2023]. We additionally use GSM8K [Cobbe et al., 2021] to evaluate the target fine-tuning performance of a given fine-tuning method. We provide a brief describe each of these evaluation metrics:

1. **HellaSwag** [Zellers et al., 2019]: A benchmark designed to test commonsense reasoning. HellaSwag presents a context followed by several plausible endings, and the model must choose the most appropriate continuation.
2. **ARC Easy** [Clark et al., 2018]: A benchmark part of the AI2 reasoning challenge designed to test basic scientific reasoning and knowledge. ARC Easy presents 5,197 multiple-choice science questions drawn from grade 3-9 standardized tests, where each question typically includes a brief scientific scenario or statement followed by four possible answer choices.
3. **ARC Challenge** [Clark et al., 2018]: A benchmark part of the AI2 reasoning challenge designed to test advanced scientific reasoning and knowledge application. ARC Challenge presents 2,590 multiple-choice science questions drawn from grade 3-9 standardized tests, where each question typically includes a scientific scenario or phenomenon followed by four possible answer choices. The questions in ARC Challenge are significantly more challenging than ARC Easy.
4. **PIQA** [Bisk et al., 2020]: A benchmark designed to evaluate physical commonsense understanding in natural language. PIQA presents a goal and two possible solutions, requiring models to choose the most appropriate solution that demonstrates an understanding of everyday physical interactions.
5. **SIQA** [Sap et al., 2019]: A benchmark designed to evaluate social commonsense intelligence and emotional reasoning. SIQA presents a social situation context followed by a question and three possible answers, requiring models to demonstrate an understanding of social interactions, emotional responses, and behavioral implications.
6. **Open Book QA** [Mihaylov et al., 2018]: A benchmark designed to assess understanding of elementary science concepts in an open-book exam format. OBQA presents 5,957 multiple-choice questions paired with a small "book" of 1,326 core science facts, requiring models to combine these facts with common knowledge to arrive at correct answers.
7. **MMLU** [Hendrycks et al., 2021b]: A benchmark designed to evaluate massive multitask language understanding. MMLU presents approximately 16,000 multiple-choice questions spanning 57 subjects including mathematics, philosophy, law, and medicine, requiring models to demonstrate broad knowledge and reasoning capabilities.
8. **MBPP** [Austin et al., 2021]: A benchmark designed to evaluate basic Python programming capabilities. The entire MBPP dataset presents 974 Python programming problems, where each problem includes a natural language task description and three test cases written as assert statements, requiring models to generate functionally correct Python code solutions.
9. **GSM8K** [Cobbe et al., 2021]: A benchmark designed to evaluate multi-step mathematical reasoning capabilities. The GSM8K test set contains 1,000 grade school math word problems,

where each problem requires 2-8 steps to solve using basic arithmetic operations (addition, subtraction, multiplication, division).

We follow the standard evaluation process for each of these datasets and specifically use lm-evaluation-harness [Gao et al., 2024] to evaluate our experiments.

G.4 Vision Implementation Details

We performed an extensive hyper-parameter search over six learning rates $\{0.05, 0.01, 0.005, 0.001, 0.0005, 0.0001\}$, two models, and six datasets (i.e., 72 total runs per method) for standard fine-tuning, linear probing, and FLOW. We chose the best learning rates associated with the highest average score over all the target (fine-tuning) datasets. Since our method is data oblivious, we do not use the validation set of ImageNet-1K other than evaluation. All vision model fine-tuning was performed on a single A6000 GPU. For fine-tuning, we used the SGD optimizer with a cosine scheduler, a weight decay of $5e - 4$ (except for the ℓ_2 -regularization baseline, where weight decay was set to 0), and a fixed random seed of 42. For fine-tuning models with ℓ_2 -regularization, we adapted the same learning rates and other related hyper-parameters used for standard fine-tuning. We searched for λ using one dataset and ResNet50 model ($\lambda = [0.002, 0.00001, 0.00002]$) and chose $\lambda = 0.002$ based on average accuracy over target data. We chose ($\alpha = 0.05$) for WiSE-FT following Wortsman et al. [2021]. We present additional training details for vision models in Table 7.

Table 7: Hyperparameter configurations for finetuning ResNet-18 and ResNet-50 on the image classification datasets.

Epochs		20	25	25	30	30	30
ResNet18	LR-Standard fine-tuning	5E-3	1E-2	5E-2	5E-3	1E-3	5E-2
	LR-Linear probing	5E-3	5E-3	5E-2	1E-2	5E-3	5E-2
	LR-FLOW	1E-3	5E-3	5E-2	1E-2	5E-3	1E-2
ResNet50	LR-Standard fine-tuning	5E-3	1E-3	1E-2	5E-3	5E-4	5E-2
	LR-Linear probing	5E-2	5E-2	5E-2	5E-2	1E-2	5E-2
	LR-FLOW	5E-4	1E-3	1E-2	1E-2	5E-3	1E-2

Datasets

1. **ImageNet-1K** [Russakovsky et al., 2015] serves as the pre-training dataset for all our vision base models. It is a widely used large-scale image classification dataset, consisting of over a million images spanning 1000 classes.
2. **CIFAR-10** [Krizhevsky, 2009] is a widely used dataset for image classification tasks. It consists of 60,000 32x32 color images divided into ten classes, with 6,000 images per class.
3. **CIFAR-100** [Krizhevsky, 2009] extends CIFAR-10 by providing 100 classes containing 600 images each. This dataset is used for fine-grained image classification tasks.
4. **Caltech101** [Li et al., 2022] comprises images of a diverse range of objects across 101 categories with a diverse set of image classes.

5. **Flowers102** [Nilsback and Zisserman, 2008] comprises 102 categories of flowers, with each category containing between 40 to 258 images. This dataset is commonly used for fine-grained image classification and flower recognition tasks.
6. **Cars** [Krause et al., 2013] refers to the Stanford Cars dataset, which includes 16,185 images of 196 classes of cars. It provides a rich resource for fine-grained car classification task.
7. **Dogs** [Parkhi et al., 2012] pertains to the Stanford Dogs dataset, containing 20,580 images of 120 breeds of dogs. This dataset is widely used for fine-grained dog breed classification and recognition tasks.

H Detailed Vision Results and Ablations

Table 8: Target accuracies on each of the six datasets for the results in Table 1.

	Method	CIFAR-10	CIFAR-100	Flowers-102	Caltech-101	Dogs	Cars	Average
ResNet18	LP	81.32	60.06	87.20	91.15	78.50	43.23	73.57
	Standard FT	96.15	83.42	92.45	94.02	80.47	87.91	89.07
	ℓ_2 -Regularization	95.53	81.82	92.11	94.23	80.27	84.78	88.12
	WiSE-FT	91.47	65.90	87.28	91.40	82.48	62.88	80.23
	FLOW (Ours)	88.25	78.95	90.01	93.05	86.20	67.17	83.93
ResNet50	Linear probing	86.62	67.80	83.64	93.45	85.76	41.97	76.45
	Standard FT	97.61	86.11	91.74	96.02	89.26	89.94	91.78
	ℓ_2 -Regularization	97.50	85.77	91.67	95.85	89.29	89.42	91.58
	WiSE-FT	94.65	72.55	71.95	93.73	92.52	62.89	81.38
	FLOW (Ours)	91.11	79.42	86.78	94.45	91.16	74.59	86.25

Table 9: Top-1 ImageNet-1K accuracy of vision models after fine-tuning on target datasets for the results in Table 1.

	Method	CIFAR-10	CIFAR-100	Flowers-102	Caltech-101	Dogs	Cars	Average
ResNet18	LP	69.76	69.76	69.76	69.76	69.76	69.76	69.76
	Standard FT	19.93	0.39	6.48	34.17	56.38	0.17	19.58
	ℓ_2 -Regularization	37.86	29.86	19.34	46.67	58.34	16.64	34.78
	WiSE-FT	62.24	47.65	49.98	64.70	67.34	33.03	54.15
	FLOW (Ours)	69.02	52.64	67.80	68.32	67.78	65.74	65.21
ResNet50	Linear probing	79.02	79.02	79.02	79.02	79.02	79.02	79.02
	Standard FT	16.89	35.95	61.01	40.51	66.93	0.21	36.91
	ℓ_2 -Regularization	33.98	47.16	62.85	43.42	67.03	14.27	44.78
	WiseFT ($\alpha = 0.5$)	61.40	73.04	76.33	73.25	77.36	8.55	61.65
	FLOW (Ours)	78.26	75.13	78.60	73.38	78.55	72.64	76.09

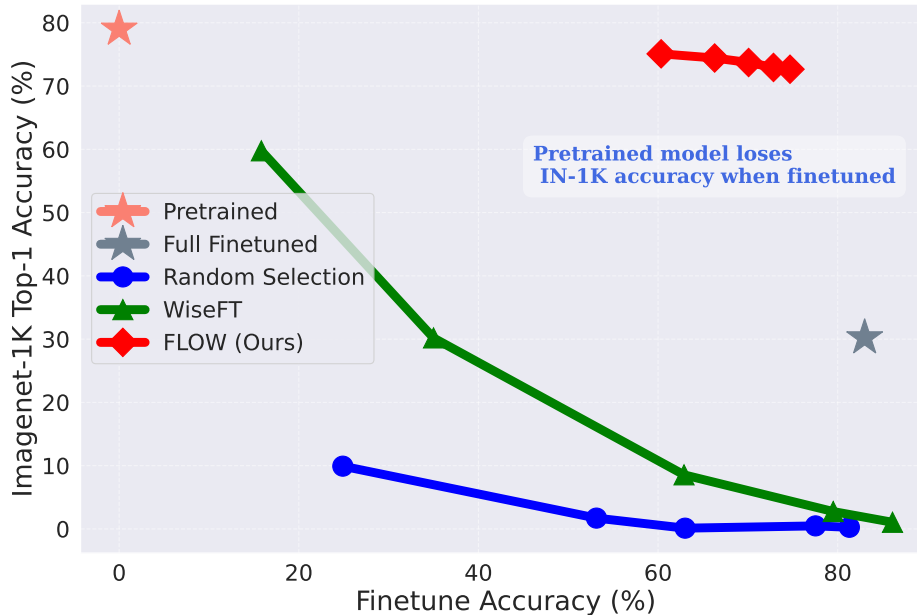


Figure 2: **Comparison of FLOW with different values of τ and other baselines also with different hyper-parameter values.** This plot is for ResNet-50 on the Stanford cars dataset. FLOW’s plot (in red) is with $\tau = \{10, 20, 30, 40, 50\}$ percentile of the per-sample losses. As the name “random selection” may imply, we just pick a random subset of the fine-tuning data and train on this subset to limit the drift from the pre-trained model. To have some correspondence with our choice of τ for FLOW, we pick random $\{10, 20, 30, 40, 50\}$ % of the data in “random selection”. As we see, FLOW significantly outperforms other methods.

I Additional Language Model Results and Ablations

In this section, we discuss expanded results and further ablations of FLOW within our language experiments, specifically covering the following:

- Appendix I.1: An expanded table of results on commonsense reasoning tasks along with other baselines.
- Appendix I.2: An additional ablation on *token-wise* weighting scheme for fine-tuning with language data.
- Appendix I.3: An expanded set of plots and results for the combination of FLOW with weight averaging techniques such as Wise-FT [Wortsman et al., 2021].

I.1 Extended Commonsense Reasoning Results

As discussed in Section 5.2 and Appendix G.3, we evaluate FLOW and the other baselines on various commonsense reasoning tasks within fine-tuning with the procedure described in Section 5.2. We include the exact results of these evaluation metrics for various baselines and FLOW in Table 10. We also include the results of commonsense reasoning metrics for the ablation combining FLOW with LoRA and ℓ_2 in Table 11.

Table 10: **Extended commonsense reasoning metrics for FLOW and other baselines within language modeling.** The performance on commonsense reasoning evaluations when fine-tuning Gemma 2 2B and Llama 3.2 3B on MetaMathQA. We include the target domain evaluation GSM8K for convenience. The results show that FLOW can effectively mitigate catastrophic forgetting while still getting strong performance on our target fine-tuning task.

	Method	ARC-e	ARC-c	HellaSwag	PIQA	SIQA	OBQA	Average	GSM8K
Gemma 2 2B	Pre-trained	80.18	46.84	54.95	78.67	51.33	31.40	57.23	24.49
	Standard Fine-tuning	76.09	42.07	45.59	9.76	48.06	32.00	55.07	63.38
	WiSE-FT	79.55	46.42	56.43	78.24	51.08	32.00	57.28	53.30
	LoRA ($r = 64$)	77.78	44.37	54.59	76.99	50.51	29.80	55.67	60.43
	ℓ_2 -Regularization	79.08	45.99	56.21	77.20	50.97	32.60	57.01	62.85
	FLOW (Ours)	79.76	47.18	56.23	77.69	51.48	33.20	57.59	62.55
Llama 3.2 3B	Pre-trained	74.54	42.15	55.31	76.66	47.03	31.20	54.48	26.01
	Standard Fine-tuning	70.03	34.22	52.02	74.16	45.24	28.40	50.68	66.95
	WiSE-FT	75.63	40.79	55.18	76.93	47.34	31.40	54.54	57.01
	LoRA ($r = 64$)	71.38	37.88	55.01	76.55	47.39	30.40	53.10	63.84
	ℓ_2 -Regularization	73.57	38.91	54.939	76.12	47.24	30.80	53.60	66.87
	FLOW (Ours)	74.96	39.68	55.39	76.01	47.80	32.00	54.30	65.58

Table 11: **Extended commonsense reasoning metrics for combining FLOW with other baselines.** The performance on commonsense reasoning evaluations when fine-tuning Gemma 2 2B baselines in conjunction with FLOW on MetaMathQA. We include the target domain evaluation GSM8K for convenience. The results show that FLOW can effectively be used in conjunction with other methods that mitigate catastrophic forgetting.

	Method	ARC-e	ARC-c	HellaSwag	PIQA	SIQA	OBQA	Average	GSM8K
	LoRA ($r = 64$)	77.78	44.37	54.59	76.99	50.51	29.80	55.67	60.43
	LoRA ($r = 64$) + FLOW	79.50	45.39	55.27	77.31	51.18	31.80	56.74	61.49
	ℓ_2 -Regularization	79.08	45.99	56.21	77.20	50.97	32.60	57.01	62.85
	ℓ_2 -Regularization + FLOW	79.67	47.10	56.38	77.48	51.13	33.40	57.53	62.02

Table 10 shows a clear trend that FLOW, can strongly mitigate catastrophic forgetting in comparison to standard fine-tuning. For Gemma 2 2B, we can see that FLOW only has $\sim 0.8\%$ reduction in the performance of the target fine-tuning while on average maintaining the commonsense reasoning abilities of the pre-trained model, a $\sim 2.52\%$ increase over standard fine-tuning. For Llama 3.2 3B, we can see that FLOW can again maintain the commonsense reasoning abilities of the base pre-trained model while only having a $\sim 1.4\%$ drop on target fine-tuning performance. Overall, FLOW strikes a strong balance between general capabilities and target fine-tuning performance compared to other baselines.

For experiments with Gemma 2 2B, FLOW can on average maintain the best scores on commonsense reasoning tasks. Performing only $\sim 0.8\%$ and $\sim 0.3\%$ worse on GSM8K in comparison to standard fine-tuning and ℓ_2 regularization, FLOW can improve on commonsense reasoning metrics by $\sim 2.42\%$ and $\sim 0.58\%$ respectively. Interestingly, in our Llama 3.2 3B experiments, we found that WiSE-FT performed the strongest in preventing catastrophic forgetting of commonsense capabilities (+0.04 over the pre-trained model); however, this came at the cost of a significant decrease in GSM8K accuracy (-9.94 under standard fine-tuning). In comparison, FLOW effectively mitigated forgetting in commonsense reasoning metrics (-0.18 under the pre-trained model), while achieving significantly higher accuracy in GSM8K (-1.37 under standard fine-tuning).

I.2 Token-wise Sample Weighting Ablations

In the language experiments, “sample” for FLOW can be defined as an entire sequence or an individual token. The experiments in the main paper treat a sequence as a sample; in that case, the per-sample loss is the average loss over the tokens in the sequence. We call this *sequence-wise* re-weighting. Instead, one could treat a token as a sample in which case the per-sample loss is just the token’s loss. We call this *token-wise* re-weighting. We run a small ablation on both *sequence-wise* and *token-wise* re-weighting by following a similar experimental setup as Section 5.2. We train a Gemma 2 2B on MetaMathQA and evaluate it on several general capability and target domain evaluations. The results of this experiment is in Table 12.

Table 12: The performance of Gemma 2B 2B on general capabilities metrics compared to target domain performance (GSM8K) when training on MetaMathQA. *Pre-trained* is the base model performance of Gemma 2 2B, *Standard* is the performance after full end-to-end fine-tuning, *Sequence* is our sequence sample weighting schema with FLOW, and *Token* is our token sample weighting schema with FLOW. **Bold** and underlined values indicate the **best** and second-best results respectively within each evaluation metric.

Method	ARC-e	ARC-c	HellaSwag	PIQA	SIQA	OBQA	MMLU	MBPP	GSM8K
Base	80.18	<u>46.84</u>	<u>54.95</u>	78.67	<u>51.33</u>	31.40	49.59	28.40	24.49
Standard	76.09	42.07	54.41	76.99	48.06	32.80	45.59	16.80	63.38
Sequence	<u>79.76</u>	47.18	56.23	77.69	51.48	<u>33.20</u>	<u>49.31</u>	<u>26.80</u>	<u>62.55</u>
Token	79.38	45.90	53.95	<u>78.29</u>	51.28	31.80	48.75	22.00	23.73

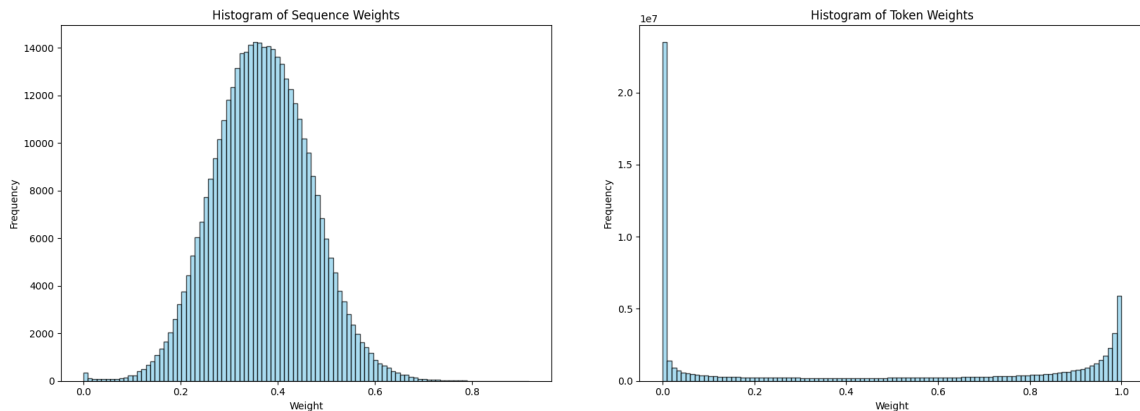


Figure 3: Histograms comparing the sample-wise distribution of weights in *sequence-wise* re-weighting schema for FLOW and token-wise distribution of weights *token-wise* re-weighting schema for FLOW. The *sequence-wise* weight distribution is given on the left, while the *token-wise* weight distribution is given on the right.

While *token-wise* sample re-weighting performs comparably or slightly worse than *sequence-wise* sample re-weighting in terms of the catastrophic forgetting of general capabilities of Gemma 2 2B, it struggles to effectively learn the fine-tuning target domain of GSM8K. To further understand this problem, we compare the weight distributions between *sequence-wise* and *token-wise* re-weighting schema in Figure 3. We can see that the *sequence* weights appear Gaussian, while most of the *token* weights are either 0 or 1. We speculate that *token-wise* re-weighting will force any token not commonly appearing in the pre-training data to have a high loss or perplexity, which combined with

our algorithm, will heavily down-weight them to almost zero. We further speculate that these tokens are essential to improving the performance of our target fine-tuning task and that using FLOW with a *token*-wise scheme over-regularizes, preventing any meaningful learning of the target task. As *sequence*-wise re-weighting significantly outperforms *token*-wise re-weighting, we recommend using *sequence*-wise re-weighting in FLOW for language models.

I.3 Extended Weight Averaging Results

As discussed in Section 6, we further combine FLOW with WiSE-FT to mitigate the effects of catastrophic forgetting when fine-tuning. In this section, we report the full results of combining FLOW and WiSE-FT to prevent catastrophic forgetting with Gemma 2 2B.

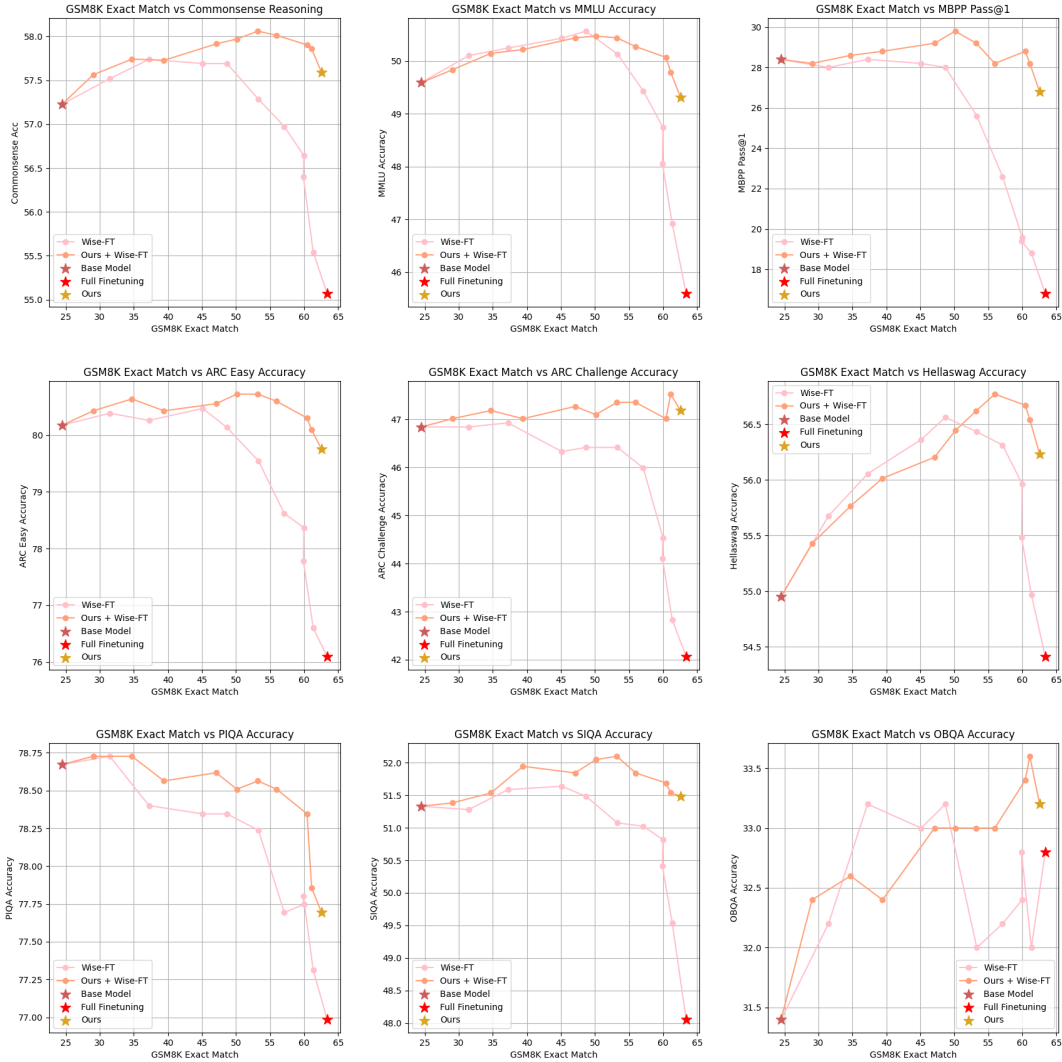


Figure 4: **FLOW** is complementary with model averaging (**WiSE-FT**) in language modeling. We compare **WiSE-FT** [Wortsman et al., 2021] with a standard model fine-tuning and with **FLOW** after fine-tuning Gemma 2 2B on MetaMathQA. We use varying $\alpha \in [0, 1]$ for **WiSE-FT**. The results indicate that combining **Wise-FT** with **FLOW** outperforms vanilla **Wise-FT** with standard fine-tuning.